INORGANIC CHEMISTRY FRONTIERS

REVIEW

View Article Online
View Journal | View Issue

Cite this: *Inorg. Chem. Front.*, 2024, **11**, 8164

Advances in nanoengineering of cathodes for next-generation solid oxide fuel cells

Chunwen Sun

In recent years, great efforts have been devoted to develop low or intermediate temperature solid oxide fuel cells (SOFCs) operating at 500–800 °C. Lowering the operating temperature can suppress degradation of components and extend the range of acceptable material selection. Moreover, this is also favorable for improving cell durability and reducing the system cost. However, reducing the operating temperature decreases the electrode kinetics and leads to large interfacial polarization resistances, especially prominent for the oxygen reduction reaction (ORR) at the cathode. This review introduces the research progress of nanoengineering of electrodes employed for SOFCs operating at low and intermediate temperatures, including nanofiber-, nanotube- and nanowire-based cathodes, nanocoatings fabricated by atomic layer deposition (ALD) and pulsed laser deposition (PLD), *in situ* exsolution nanoparticles from perovskite materials, infiltration nanoparticles, single-atom based cathode catalysts, triple-conducting oxide cathodes, *etc*. Finally, we also provide future research directions on nanoengineering of cathodes for next-generation SOFCs.

Received 27th September 2024,
Accepted 28th October 2024

DOI: 10.1039/d4qi02451f

rsc.li/frontiers-inorganic

1. Introduction

The adverse impact of conventional energy production methods like fossil fuel combustion on the environment and resource has resulted in an increased exploitation of alternative but greener and more sustainable energy sources. Fuel cells with merits of low pollutant emission and high efficiency have been regarded as a promising technology for power generation. In particular, solid oxide fuel cells (SOFCs), based on oxide-ion or proton conducting electrolytes, have several merits compared to other types of fuel cells, including relatively inexpensive materials, low sensitivity to impurities in the fuel, and high efficiency.[1–10]

SOFCs cannot yet compete with conventional combustion systems in terms of cost and durability. In recent years, great efforts have been devoted to develop low or intermediate temperature SOFCs operating at 500–800 °C.[11–13] Lowering the operating temperature can suppress degradation of components and extend the range of acceptable material selection, improve cell durability and reduce the system cost. Moreover, SOFCs operating at low temperature (LT) and intermediate temperature (IT) have shorter start-up time and economic competitiveness for a large number of applications, such as small scale portable devices, auxiliary power units for automobiles and large distributed power generation systems.[1–5] However, reducing the operating temperature simultaneously decreases the electrode kinetics and results in large interfacial polarization resistances. This effect is most prominent for the oxygen reduction reaction (ORR) at the cathode. In order to lower the polarization resistance of the cathode, favorable electronic and ionic conductivities and a high catalytic activity for the ORR are essential.

A vast number of papers related to the topic of SOFC cathodes have been published in the past decades. This review aims to provide an overview of the present research progress in the field of nanoengineering of SOFC cathodes for LT- or IT-SOFCs, including nanofiber-, nanotube- and nanowire-based cathodes, nanocoatings fabricated by atomic layer deposition and pulsed laser deposition, *in situ* exsolution nanoparticles from perovskite materials, infiltration nanoparticles, single-atom based cathode catalysts, triple-conducting oxide cathodes, and so on.

2. Overview of cathode reaction mechanisms

2.1 Cathode requirements

In SOFCs, the cathode acts as the site for the electrochemical reduction of oxygen. To this effect, the cathode must have the following properties:[2] (1) high electronic conductivity, preferably more than 100 S cm^{-1} under an oxidizing atmosphere; (2) a matched thermal expansion coefficient (TEC) and chemical compatibility with the electrolyte and interconnect materials;

School of Chemical & Environmental Engineering, China University of Mining and Technology-Beijing, Beijing 100083, P. R. China. E-mail: csun@cumtb.edu.cn

(3) adequate porosity to allow gaseous oxygen to readily diffuse through the cathode to the cathode/electrolyte interface; (4) stability under an oxidizing atmosphere during fabrication and operation; (5) high catalytic activity for the oxygen reduction reaction (ORR); and (6) low cost. For high temperature SOFCs operating typically at 800–1000 °C, the cathode material of choice is a composite of Sr-doped $LaMnO_3$ (LSM) and yttria-stabilized zirconia (YSZ). For LT- and IT-SOFCs, mixed ionic-electronic conductors (MIECs) and triple conducting ($H^+/O^{2-}/e^-$) oxide (TCO) cathodes are preferable.

The operating temperature of SOFCs is determined by the temperature required to achieve sufficient ionic conductivity in the electrolyte. For example, given that the electrolyte should not contribute more than 0.15 Ω cm^2 to the total area-specific resistance (ASR) of the cell, for a electrolyte film with a thickness of 15 μm, its ionic conductivity should exceed 10^{-2} S cm^{-1} at the operating temperature.[3] In addition, the choice of cathode materials is largely dependent on the electrolyte materials used, with care taken to match thermal expansion coefficients and avoid undesirable interface reactions.[2] The most commonly used electrolyte material is YSZ. Other oxides, such as scandia-stabilized zirconia (ScSZ), samaria doped ceria (SDC), gadolinia doped ceria (GDC), and lanthanum strontium gallium magnesium oxide (LSGM), are also under consideration because they have higher ionic conductivities at reduced operating temperatures. The TEC and ionic conductivity of various electrolyte materials used commonly can be referred to in our previous review paper.[2]

Chunwen Sun

Prof. Chunwen Sun received his Ph.D. degree in Condensed Matter Physics from the Institute of Physics (IOP), Chinese Academy of Sciences (CAS) in 2006. He is a full professor and group leader of Energy Storage Materials and Devices at the School of Chemical and Environmental Engineering at the China University of Mining & Technology (Beijing). He is also the director of Joint Laboratory on Energy Materials between China and Spain, supported by the National Key R&D Program of China and the Ministry of Science and Innovation, Spain. His research interests include solid oxide fuel cells, solid oxide electrolyzers, lithium-ion batteries, all-solid-state batteries and electrocatalysis. He has published 190 peer-reviewed papers with more than 18 000 citations (Google Scholar), edited 9 book chapters and filed 26 Chinese patents. He has also received a number of awards, including the Outstanding Overseas Talents by the Institute of Physics CAS (2011), the International Association of Advanced Materials (IAAM) Scientist Medal (2017), the Chinese Most Cited Researchers for exceptional research performance in the field of Materials Science and Chemistry, Elsevier (2018–2023), and The Most Influential Paper Award of Chinese Physics Society in 2020.

2.2 Triple-phase boundaries at cathodes

On the surface of the cathode, the oxygen reduction can be described as follows:

$$\frac{1}{2}\,O_2\ (\text{gas}) + 2e^-(\text{cathode}) \rightarrow O^{2-}(\text{electrolyte}) \qquad (1)$$

The electrochemical reactions are quite different from normal heterogeneous reactions in many aspects.[14] It is widely believed that the electrochemical reactions can only occur at the triple-phase boundaries (TPBs), which are defined as the confluence sites where the oxygen ion conductor, the electronic conductor, and the gas phase come in contact. A schematic illustration of the region between the electrolyte and the cathode where the TPB exists is shown in Fig. 1a. If there is a breakdown in connectivity in any one of the three phases, the reaction cannot occur.[15] Moreover, a hindrance of access for ions, gases or electrons to the reaction site renders it inactive. The microstructure and composition significantly influence the size and distribution of the TPBs. One compositional design option employed is to provide a single phase electrode with mixed conductivities, allowing both oxide ion and electron mobility within the cathode material, *e.g.*, $La_{1-x}Sr_xCo_{1-y}Fe_yO_{3-\delta}$ (LSCF), or with triple-conducting oxides for proton conducting electrolyte-based SOFCs, *e.g.*, $PrNi_{0.5}Co_{0.5}O_{3-\delta}$. Thus, electrochemical oxygen reduction can occur at the electrode surface as well as within the bulk electrode. Another strategy is to use a porous composite consisting of an electronic conducting cathode material and an appropriate amount of ionic conducting electrolyte material, *e.g.*, LSM–YSZ. By using these strategies, the electrochemically active reaction sites can be increased by orders of magnitude compared with those of porous cathodes exhibiting only electronic conductivity. The degree of this extension depends critically on the rate of defect transport through the solid MIECs, gas transport through the pores to promote surface coverage in the MIECs, and the catalytic activity of interfaces.

2.3 Kinetics and reaction mechanisms of cathodes

Although the molecular species involved in the overall electrochemical reactions at the cathode is an O_2 molecule, it must first be converted to some "electroactive" intermediate species *via* one or more processes. Usually, this electrochemically kinetic step is restricted to an area close to TPBs.[16,17] The electrochemical processes going on in the cathode involve different bulk and surface steps.[15,17,18] The elementary reactions in the overall electrode reaction are usually considered as follows:[19,20] (i) the reduction of O_2 molecules, involving adsorption, dissociation, reduction, and incorporation of the oxygen anion into the lattice of the cathode materials; (ii) ionic transport through the porous cathode toward the electrolyte; and (iii) the ions jumping into the electrolyte lattice. Among all three elementary reaction steps, several steps could be rate-limiting for the ORR process. The oxygen reduction step is the

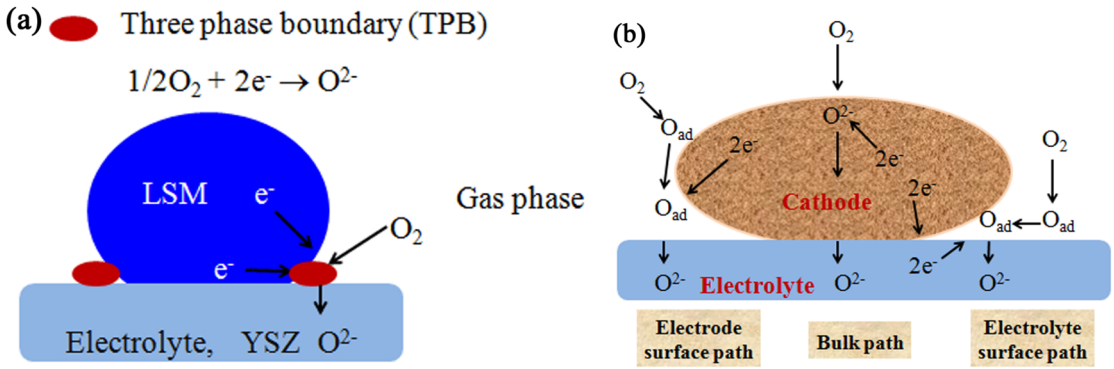

Fig. 1 (a) Schematic diagram of the cathode triple-phase boundary. (b) Schematic of the proposed reaction pathways in the literature for the oxygen reduction reaction.

biggest contributor to total cell resistance, and improvements in the catalytic activity of the cathode have a strong impact on the final cell performance.[21,22]

For electron-conducting perovskite-type materials, there are three possible paths for the cathodic ORR, that is, the electrode surface path, the bulk path, and the electrolyte surface path, as schematically illustrated in Fig. 1b. These three paths are in sequence suitable for the cases of an electronic conductor (*e.g.*, LSM), a MIEC conductor (*e.g.*, LSCF), and a composite (*e.g.*, LSM–YSZ), respectively.

The cathodic reaction can simultaneously occur *via* all three paths, and for each path, one or more elementary steps determine the corresponding reaction rate.[23] Which elementary reaction will be rate limiting step is not always predictable and may depend on local conditions like temperature and oxygen partial pressure, or on microstructural conditions. In addition, there may be parallel reaction pathways, and a crossover of these various reaction pathways may cause interference. For example, the incorporation rate into the cathode (bulk path) depends on the surface concentration of adsorbed oxygen and thus can be affected by the surface diffusion occurring *via* the electrode surface path mechanism.

To reduce the operating temperature of SOFCs from 800 to 500 °C, two major challenges must be addressed. One is decreasing the high ohmic resistance without decreasing the electrolyte thickness below 5 mm. Thus, ceria-based electrolytes of $Ce_{1-x}M_xO_{2-\delta}$ (M = Gd and Sm, $x \leq 0.2$) are regarded as the most suitable for LT-SOFCs, owing to their high ionic conductivity of 20 mS cm^{-1} at 650 °C.[24] In addition, they are chemically compatible with most of the cathode materials. An alternative candidate is $La_{0.8}Sr_{0.2}Ga_{0.8}Mg_{0.2}O_{3-\delta}$ (LSGM) with a high ionic conductivity of 33 mS cm^{-1} at 650 °C in the intermediate temperature range from 600 to 800 °C, but it is difficult to synthesize and the high cost of gallium hinders its application.[25,26] Another challenge is development of high-performance cathodes compatible with the electrolyte material. The electrode polarization losses are usually associated with the generation and transport of oxygen ions within the porous cathode structure.[27] The Adler or ALS model[28] could provide a strategy for optimizing the composition and structure of electrodes to obtain good performance at low and intermediate temperatures.

3. Development of nanostructured cathodes

At reduced operating temperatures, SOFC resistance increases rapidly and is often dominated by the interfacial polarization resistance between the electrolyte and the cathode. Accordingly, the SOFC resistance could be substantially reduced by developing novel cathode materials and/or unique microstructures to lower the interfacial polarization resistance.[29–33] To date, several new electrode architectures have been used to achieve high SOFC performances at low temperatures. Among these, nanostructured electrodes are most attractive since the microstructures at the nanoscale enable available larger TPBs and more active sites for the electrocatalytic processes of oxygen reduction.

3.1 Nanofiber-, nanotube- and nanowire-based cathodes

Electrospinning is a commonly used and promising method to prepare one-dimensional (1D) nanofibers and nanotubes with a small average diameter, a high specific surface area, and high porosity, which can greatly enhance the electrocatalytic activity of the electrodes. Recently, Liu *et al.*[35] reviewed the research progress of electrospinning technology in the SOFC field.

The 1D $La_{0.8}Sr_{0.2}Co_{0.2}Fe_{0.8}O_{3-\delta}$ (LSCF)/$Ce_{0.8}Gd_{0.2}O_{1.9}$ (GDC) nanocomposite was prepared by an electrospinning technique and a multi-step infiltration process, and demonstrated to be a good candidate for IT-SOFC cathodes.[34] The polarization resistance of the nanorod structured LSCF/GDC cathode with 160 mL GDC loading was 5 times smaller than that of the LSCF/GDC nanoparticle (NP) composite cathode with an optimal GDC loading of 80 mL under identical testing conditions, which was attributed to its unique structure with a larger LSCF/GDC boundary length and higher porosity. Similarly, Zhi *et al.*[36] fabricated LSCF nanofibers using the electrospinning method and used them as the cathode for YSZ electrolyte-based IT-SOFCs. The fuel cell with the monolithic

LSCF nanofiber cathode exhibited a power density of 0.90 W cm^{-2} at 1.9 A cm^{-2} at 750 °C. Furthermore, the electrochemical performance of the cell was improved by infiltration of 20 wt% of GDC into the LSCF nanofiber cathode. The cell with the LSCF–20% GDC composite cathode showed a power density of 1.07 W cm^{-2} at 1.9 A cm^{-2} at 750 °C. To improve the electron transfer and enhance active sites for the ORR in the cathode, $La_{0.8}Sr_{0.2}MnO_3$–YSZ nanofibers with porosity of up to 50% were co-spun by the electrospinning method,[37] which significantly reduced the resistance of mass transfer and enhanced the electron and ion transport.

$Sm_{0.5}Sr_{0.5}CoO_{3-\delta}$ (SSC) is an excellent cathode for IT-SOFCs.[38] SSC nanowires with 20–100 nm diameters were prepared by electrospinning.[39] The ASR of the electrolyte/nanofiber-electrode reached 0.533 and 0.010 Ω cm^2 at 500 and 700 °C, respectively. The single cell consisting of the NiO-CGO/CGO/SSC nanofiber displayed a peak power density of 1.09 W cm^{-2} at 700 °C.

Porous cobaltite $La_{0.6}Sr_{0.4}CoO_3$ nanotubes were prepared by Bellino *et al.*[40] using a pore wetting method. As a cathode for IT-SOFCs, they showed a low ASR of 0.21 Ω cm^2 at 700 °C. The effect of the diameter of the precursor nanotubes on the polarization resistance of the $La_{0.6}Sr_{0.4}CoO_3$ (LSCO) cathodes on CeO_2–10 mol% Sm_2O_3 (SDC) electrolytes under an air atmosphere was further evaluated in symmetrical LSCO/SDC/LSCO cells by Sacanell *et al.*[41]

3.2 Nanocoatings fabricated by atomic layer deposition and pulsed laser deposition

Atomic layer deposition (ALD) can realize precise nanoscale design, owing to its ability for atomic-level control over the nanostructure and composition. In a perspective article published by Asundi *et al.*,[42] they reviewed applications of ALD in improving the performance of materials for energy capture, storage, and consumption; the long-term stability of a conventional MIEC cathode of the $La_{0.6}Sr_{0.4}Fe_{0.8}Co_{0.2}O_{3-\delta}$-$Gd_{0.2}Ce_{0.8}O_{1.9}$ (LSCF–GDC) composite was improved by functionalizing its surfaces with a conformal layer of nanoscale ZrO_2 films through ALD.[43] The overcoated LSCF–GDC cathode exhibited polarization and ohmic ASR 3 and 1.5 times lower than those of the pristine sample for >1100 h testing at 800 °C, while the pristine LSCF–GDC cathode decayed at a 4 times faster rate. The multifunctionality of porosity, mixed conductivity, and suppressed Sr-enrichment enabled by the nanoscale ALD-ZrO_2 overcoats were attributed to the performance retention observed for the overcoated cathode. Similarly, as a highly active but unstable IT-SOFC cathode, $La_{0.6}Sr_{0.4}CoO_{3-\delta}$ (LSCo) was also coated on its surfaces with a conformal layer of nanoscale ZrO_2 films through ALD, which exhibited high ORR activity with exceptional stability for 4000 h at 700 °C.[44] The unique multifunctionality of the ALD-derived nanoscale ZrO_2 overcoats, that is, possessing porosity for O_2 access to LSCo, conducting both electrons and oxygen ions, confining thermal growth of LSCo nanoparticles, and suppressing surface Sr segregation, contributed to the durable and highly active nanostructured cathode.

Pulsed laser deposition (PLD) technology has been utilized to explore alternative and nanoengineered cathode materials exhibiting high performance in terms of low ASR and high oxygen exchange properties superior to those of conventional cathodes prepared by screen-printing techniques.[45–47] Develos-Bagarinao *et al.*[48] reported an innovative concept for preparing high-performance thin-film cathodes comprising nanoporous $La_{0.6}Sr_{0.4}CoO_{3-\delta}$ cathodes in conjunction with highly ordered, self-assembled nanocomposite $La_{0.6}Sr_{0.4}Co_{0.2}Fe_{0.8}O_{3-\delta}$ and $Ce_{0.9}Gd_{0.1}O_{2-\delta}$ cathode layers using pulsed laser deposition (PLD), as shown in Fig. 2a and b. Integration of the nanoengineered cathode layers into conventional anode-supported cells enabled the achievement of high current densities of ~2.2 and ~4.7 A cm^{-2} at 0.7 V at 650 °C and 700 °C, respectively (Fig. 2c). This cell also exhibited a low ohmic resistance R_{ohm} of 0.026 Ω cm^2 and polarization resistance R_p of 0.030 Ω cm^2 under an operating condition of 0.75 V, as shown in Fig. 2d, which are attributed to the utilization of a thin YSZ electrolyte and dense GDC interlayer, and high oxygen exchange properties ascribed to the nanoengineered cathode layers, respectively. These results demonstrate that modulating material properties through an effective approach could significantly boost the electrochemical performance of cathodes for IT-SOFCs.

$Ba_{0.5}Sr_{0.5}Co_{0.8}Fe_{0.2}O_{3-\delta}$ (BSCF) is an excellent cathode material for reduced temperature SOFCs. Liu *et al.*[49] fabricated a BSCF thin cathode on the YSZ/NiO-YSZ composite substrate by the PLD technique. The electrochemical performance of the cathode deposited by PLD outperformed that based on the screen-printing method. The maximum power density of the cell made using PLD reached 1.12 W cm^{-2} at 800 °C, compared to that of 0.45 W cm^{-2} of the cell fabricated by the screen-printing method. This enhancement was mainly ascribed to the smaller internal resistance within the cathode and the interfacial resistance between the cathode and the electrolyte. These results indicated that the PLD film-deposition approach could enable a significant improvement of the interfacial contact between the cathode and the YSZ electrolyte.

Among various approaches for depositing oxide thin films, pulsed laser deposition and atomic layer deposition play an important role in fabricating thin, bilayered electrolytes as well as cathode and anode functional layers for achieving high power densities and durability due to their ability for control over the nanostructure and composition. However, for industrial applications, cost-effective technologies are still highly desired to be developed.

The possibility of incorporating ALD or PLD with faster deposition rates, design flexibility, and easy scalability makes them promising and attractive for SOFC applications. There is a lot of work to be done to scale up the manufacturing process either by combining existing techniques or by developing new ones, and active collaboration between academia and industry is necessary to drive future innovations. There is no doubt that ALD and PLD have a bright future in fabricating next-generation SOFCs.

In summary, although the benefits of producing particles with tailored interfaces using the ALD technique have been

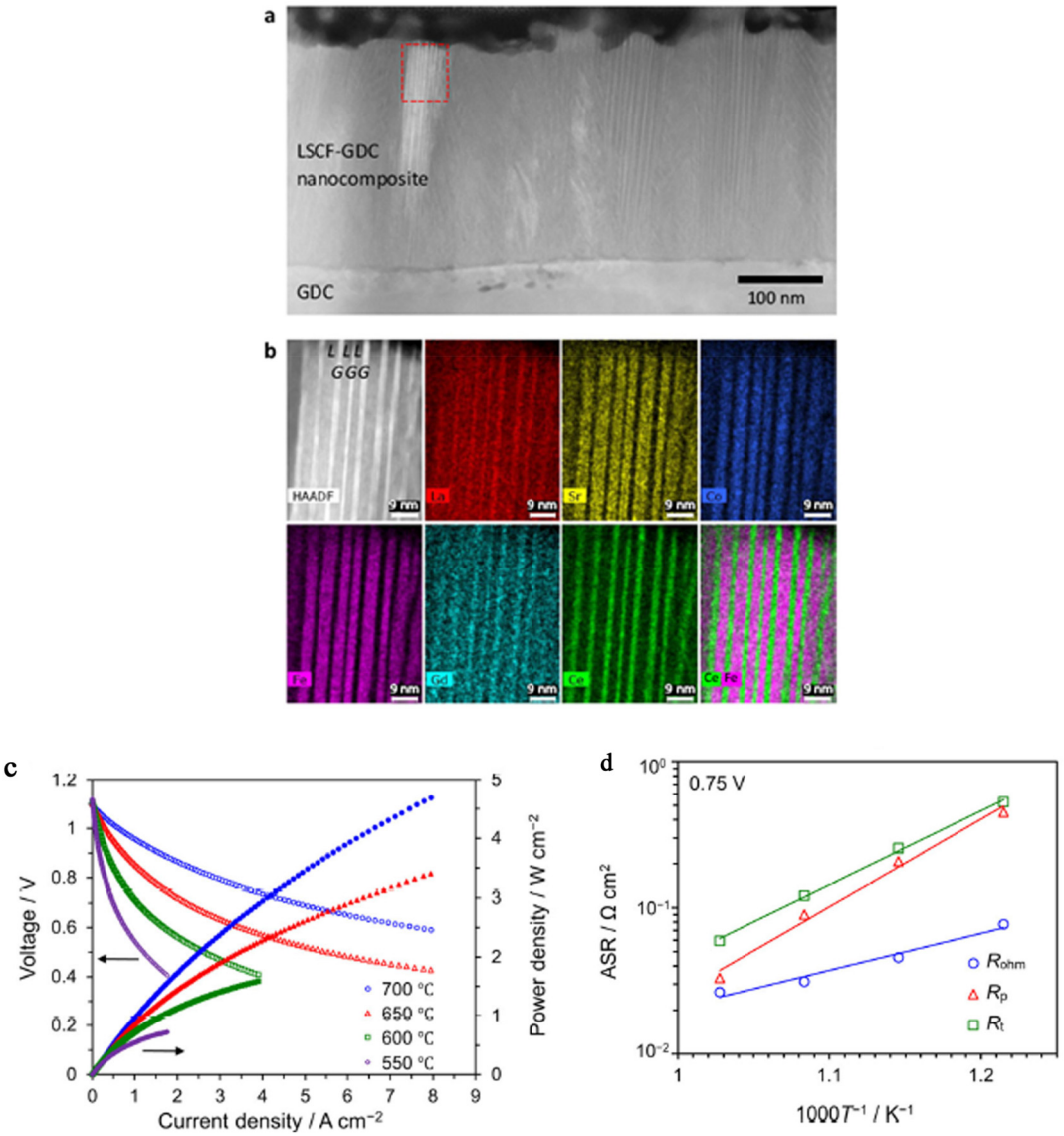

Fig. 2 Microstructure and phase distribution of the LSCF–GDC nanocomposite film, reprinted from ref. 48 with permission from Nature Publishing Group. (a) A low-magnification STEM-HAAD image showing the existence of self-assembled nanostriped patterns with long-range ordering across the thickness of the LSCF–GDC nanocomposite film. (b) STEM-HAADF and STEM-EDX elemental distributions of the various elements comprising LSCF (La, Sr, Co and Fe) and GDC (Gd and Ce) phases within the area denoted by a dashed rectangle in (a). On the STEM-HAADF image, LSCF and GDC regions are marked by L and G, respectively. (c and d) Electrochemical performance of the anode-supported cell. This cell with a nanoengineered cathode layer comprising nanoporous LSC and LSCF–GDC nanocomposites was tested using 3% H_2O humidified H_2 as the fuel and dry air as the oxidant at various temperatures (700 °C: blue circles, 650 °C: red triangles, 600 °C: green squares, 550 °C: purple diamonds). (c) *I–V* and *I–P* curves tested at different temperatures. (d) ASRs for the anode-supported cell as determined from the impedance spectra (R_p: polarization resistance, R_{ohm}: ohmic resistance, R_t: total resistance).

widely demonstrated in the field of energy storage, electrophoresis (EP) and electrostatic spraying (ES) have also gained much attraction for large-scale manufacturing of SOFCs, especially for fabricating the electrolyte on metal-supported SOFCs on a commercial scale using the ES process. In addition, the dip-coating method is one of the most cost-effective wet-coating processes,[50–53] but accurate thickness control and thin layer fabrication are limited. Furthermore, spray pyrolysis has also demonstrated to be an economical approach to prepare nanostructured electrodes with different architectures, offering the following advantages over the conventional methods: (i) simple, automatable and industrially scalable process; (ii) preparation of layers in a single deposition step, reducing time and fabrication costs; and (iii) highly reproducible process over large areas.[54]

3.3 *In situ* exsolution nanoparticles from perovskite materials

Usage of *in situ* exsolution nanoparticles from perovskite materials has been demonstrated to be an effective surface

modification approach to facilitate good control over the size and distribution of the exsolved particles by adjusting the temperature and time under a reducing atmosphere. Importantly, the exsolved nanoparticles exhibit excellent resistance to agglomeration due to the strong interaction between the support and nanoparticles.[55] Therefore, a large number of efficient nanoparticle-modified perovskite catalysts were obtained by *in situ* exsolution.[49–51] However, it should be pointed out that most of them were anode materials among these exsolved catalysts in SOFCs. Only a few cathode materials modified by *in situ* exsolved nanoparticles have been reported so far. This is mainly due to the fact that the cathode material is under an oxidizing atmosphere, and the exsolved metal nanoparticles are easily reoxidized and dissolved back into the perovskite lattice.[56]

Unlike the case that exsolution of nanoparticles are obtained in a reducing atmosphere in the anode, the exsolved nanoparticles can be achieved in the cathode by applying a negative voltage. Taking an example, the ORR activity of rare earth-doped $Ln_{0.2}Ba_{0.8}Co_{0.7}Fe_{0.3}O_{3-\delta}$ (Ln = La, Pr, Nd) cathodes below 600 °C was significantly enhanced through the exsolution of highly active nanoparticles driven by applying a negative voltage of 2 V for 150 s.[57] It revealed that voltage-driven reduction can produce nanoparticles similar to the common exsolution by hydrogen reduction in the anode, enabling the cathode to exhibit superior catalytic activity towards the ORR. Zhang *et al.*[58] reported the study of the manipulation of rare earth-doped cathodes on a voltage-driven exsolution process of perovskite cathodes. The ORR activity of rare earth-doped $Ln_{0.2}Ba_{0.8}Co_{0.7}Fe_{0.3}O_{3-\delta}$ (Ln = La, Pr, Nd) cathodes below 600 °C was significantly enhanced through the exsolution of highly active nanoparticles driven by applying a voltage. In particular, the $Pr_{0.2}Ba_{0.8}Co_{0.7}Fe_{0.3}O_{3-\delta}$ (PBCF) cathode exhibited an ASR of ~0.119 Ω cm^2 at 550 °C, approximately one-third of that for the pristine cathode (~0.389 Ω cm^2). Such an improvement was ascribed to the modification of its surface with high-density and small-size CoO nanoparticles. Furthermore, the voltage-driven exsolution process can be manipulated by the surface oxygen vacancy concentration induced by rare earth doping. Compared with La- and Nd-doped cathodes, the PBCF cathode had a higher surface oxygen vacancy concentration, promoting the exsolution of Co in the bulk and resulting in the formation of higher density and smaller size nanoparticles. This negative voltage driven strategy may provide a new approach for designing high-performance catalysts for LT-SOFCs.

For proton-conducting SOFC application, new $Pr_{0.5}Sr_{0.5}MnO_{3-\delta}$ (PSM50)-PrO_{2-x} composite cathodes were developed by Zhou *et al.*[59] The exsolution of PrO_{2-x} particles was verified by structure analysis and morphology observations. It was found that the amount of exsolved PrO_{2-x} increased with the amount of Pr in $Pr_xSr_{0.5}MnO_{3-\delta}$. The construction of a PSM50/PrO_2 heterostructure interface can reduce the formation energy of oxygen vacancies, hence accelerating the ORR kinetics of the cathode, as confirmed by oxygen diffusion and surface exchange experiments.

Symmetrical SOFCs with a redox stable material as both the anode and cathode have the following merits:[60] Possible sulfur poisoning or coke formation on the surface of the anode can be eliminated by operating the anode as a cathode; air as an oxidant will flush any sulfur or carbon species absorbed on the electrode, thereby regenerating the electrode from sulfur or coke deactivation. Moreover, a redox stable cathode can also enhance the cathode durability since oxygen partial pressure at the TPB region of the cathode can be quite low, especially when SOFCs are operated at a low cell voltage (*e.g.*, to achieve very high current density). We reported a rational design of a very active Ni-doped $La_{0.6}Sr_{0.4}FeO_{3-\delta}$ (LSFN) symmetric electrode for hydrocarbon-fueled SOFCs.[61] Homogeneously dispersed Ni–Fe alloy nanoparticles with an average diameter of ~20 nm were *in situ* extruded to the surface of the LSFN particles during the operation conditions of the cell (Fig. 3a–e). Symmetric SOFC single cells were prepared by impregnating an LSFN precursor solution into a YSZ monolithic cell as well as by a subsequent heat treatment. The single cell showed excellent output and durability in hydrocarbon-based fuels at 750 °C, as shown in Fig. 3f–h.

One of the strong advantages of the ex-solved catalysts is their superior chemical/thermal durability even under harsh high-temperature operating conditions. However, unlike achieving exsolution of an anode material operating under a reducing atmosphere, the exsolved nanoparticles can only be accomplished by applying a negative voltage in the cathode.

3.4 Infiltration of nanoparticles

Nanoscale engineering of electrode structures *via* metal salt solution impregnation or infiltration has gained increasing attention as the most effective way to develop highly active and advanced electrode structures for SOFCs. In this process, a porous electrolyte backbone is normally formed on a dense electrolyte, and then a precursor solution containing stoichiometric metal salt precursors of the catalyst material is infiltrated into the porous backbone.[62–64] After successive infiltration/thermal treatments, a nanostructured electrode is formed on the backbone surface. In this way, electrodes with an extended TPB length were obtained, and were more efficient at low operating temperatures. Jiang[62] reviewed the advances and challenges in the development of nanoscale and nanostructured electrodes and the fundamental understanding of the remarkable enhancement in the electrode performance.

The infiltrated catalytic nanoparticles can form a discrete distribution or a thin and continuous network on the surface of the porous scaffold, as schematically shown in Fig. 4a–c. The porous scaffold can be electronic conducting electrode materials (*e.g.*, LSM) or ionic conducting electrolyte materials (*e.g.*, YSZ and doped ceria). The latter requires deposition of a continuous nanoparticle layer with high electronic conductivity as well as high electrocatalytic activity, and multiple infiltration steps are necessary to achieve sufficient electron conduction.[65–69] A novel active cathode structure of $La_{0.6}Sr_{0.4}Fe_{0.9}Sc_{0.1}O_{3-\delta}$ (LSFSc) infiltrated porous YSZ was prepared by tape casting, co-sintering and infiltration techniques by Wang *et al.*[67] As shown in Fig. 4d, the infiltrated LSFSc nanoparticles catalyst was coated onto the internal surface of

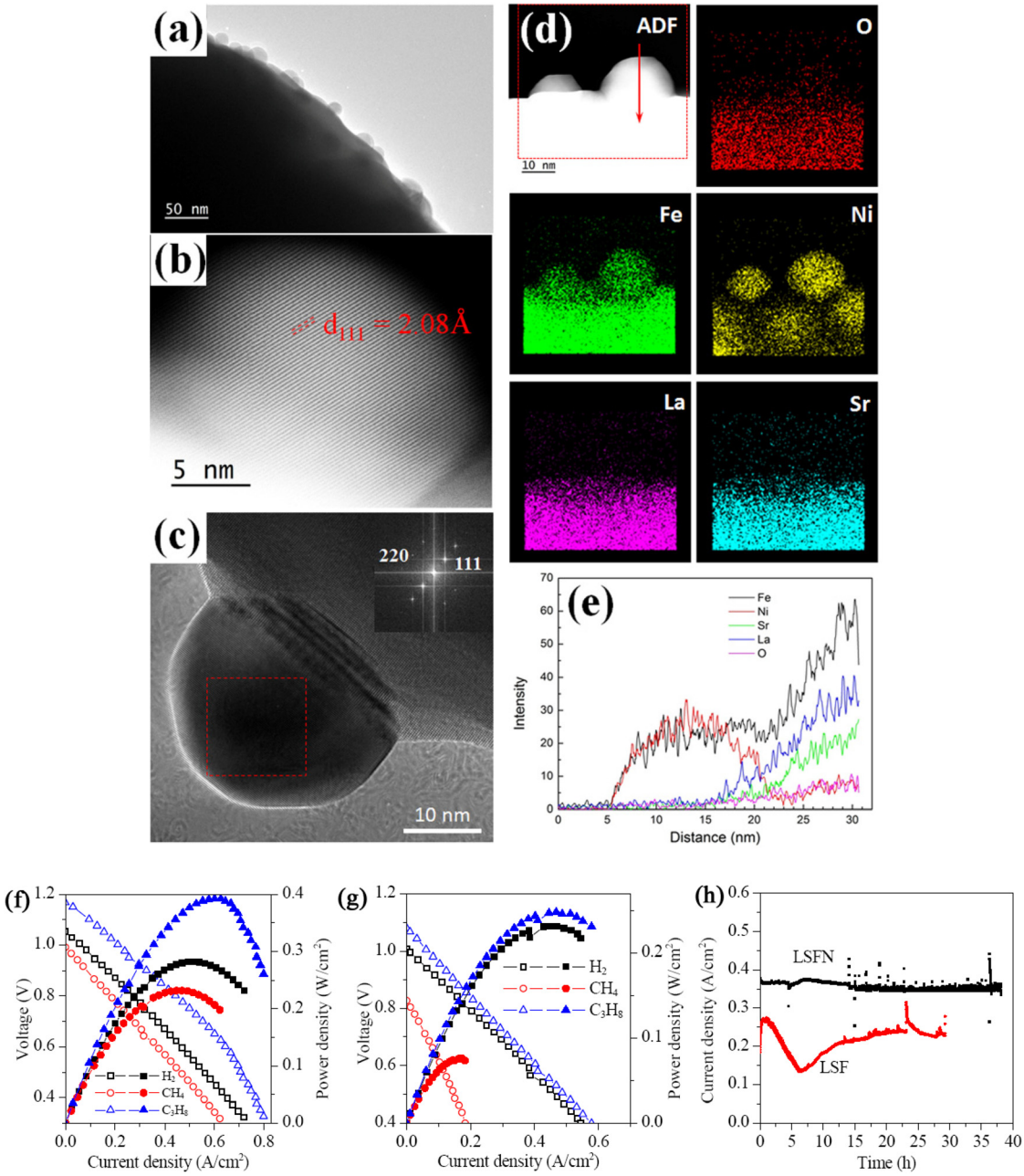

Fig. 3 TEM images of the reduced $La_{0.6}Sr_{0.4}Fe_{0.9}Ni_{0.1}O_{3-\delta}$ powder. (a) Low magnification. (b and c) High magnification; inset: the FFT pattern taken from the marked area. (d) ADF STEM image and the corresponding EDS elemental mappings. (e) The corresponding EDS line-scanning profiles along the arrow shown in (d). (f and g) Cell voltage (left) and power density (right) as a function of the current density for the monolithic cell with different electrodes: (f) LSFN and (g) LSF. (h) Current densities measured at 750 °C in C_3H_8 as a function of time for the cell with different electrodes operated at a constant voltage of 0.7 V in humidified C_3H_8, reprinted from ref. 61 with permission from Elsevier Ltd.

the porous YSZ backbone. The well-connected particles provide sufficient electron-conducting networks and numerous TPBs for the ORR without high temperature sintering. The cell with this cathode active layer (CAL) and Ni/SDC anode showed peak power densities of 0.574, 0.733 and 0.835 W cm^{-2}, respectively, with H_2 as the fuel and air as the oxidant, as shown in Fig. 4f. The polarization resistance of the cell with CAL is only 0.324 Ω cm^2 at 800 °C (Fig. 4g), which is much smaller than the reported results in the literature studies. Such a repeated infiltration process is time-consuming and hinders its practical application. Sholklapper *et al.*[68] showed that it may be possible to form a continuous and thin nano-structured LSM layer on the YSZ scaffold with a single-step infiltration process using a concentrated LSM nitrate precursor solution with a surfactant (*e.g.*, Triton X-100). The infiltrated LSM nanoparticles formed a continuous layer on YSZ particles with a thickness of 30–100 nm (~6 wt% of the YSZ scaffold). However, it is very difficult for concentrated precursor solu-

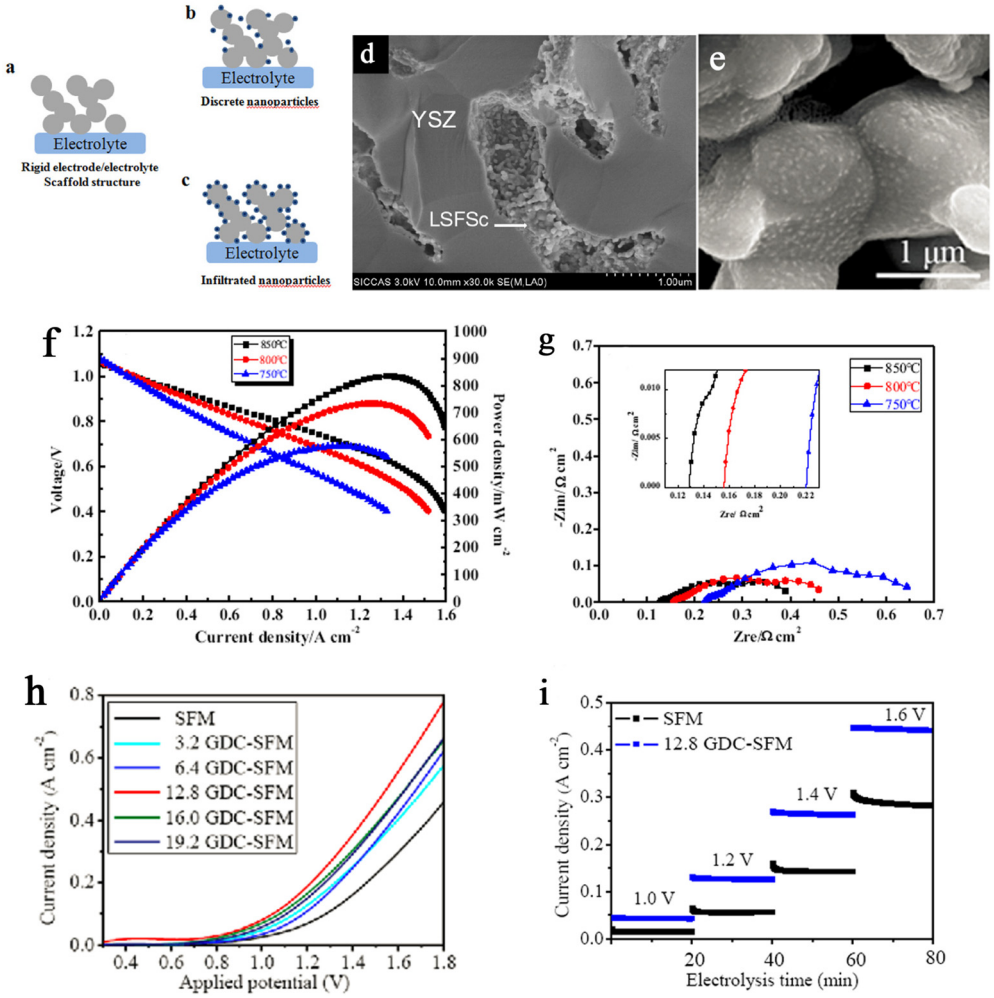

Fig. 4 (a–c) Schematic illustration of the infiltrated nanostructure electrodes on a pre-sintered porous electrode or an electrolyte scaffold. (d) High-magnification SEM image of the impregnated LSFSc-YSZ cathode, reprinted from ref. 67 with permission from Elsevier Ltd. (e) SEM image of $Sr_2Fe_{1.5}Mo_{0.5}O_{6-\delta}$ infiltrated 12.8 wt% GDC composite cathodes, reprinted from ref. 70 with permission from Elsevier Ltd. (f and g) Electrochemical performance of the cell with the CAL and Ni/SDC anode, reprinted from ref. 67 with permission from Elsevier Ltd. (h) *I–V* curves of the cells at 800 °C. (i) Potentiostatic tests of SOECs with the SFM and 12.8 wt% GDE-SFM cathodes at various voltages and 800 °C, reprinted from ref. 70 with permission from Elsevier Ltd.

tions to penetrate and infiltrate uniformly into micro- and nanopores of the scaffold due to the capillary force even under a vacuum treatment, and multiple infiltration-calcination steps are normally required, particularly in the case of thick anode substrate supports. The resistance comparison of the cells with the pristine cathode and with the infiltrated cathode showed that the infiltrated cell has a much lower ohmic resistance (R_{ohm}) of ~0.3 Ω cm^2 than that of the non-infiltrated cell (~3.4 Ω cm^2). Considering another example, Fig. 4e shows the SEM image of $Sr_2Fe_{1.5}Mo_{0.5}O_{6-\delta}$ (SFM) infiltrated 12.8 wt% GDC composite cathodes.[70] Fig. 4h shows typical current–voltage (*I–V*) curves for CO_2RR using the SFM cathodes infiltrated with various amounts of GDC at 800 °C. The current densities of the GDC–SFM cathodes increase steeply with increasing applied voltages above 1.0 V, indicating that the infiltration of GDC could greatly enhance the cell performance for CO_2RR compared with the pristine SFM cathode. In addition, the CO_2RR performance first increases with increasing the GDC loading amount to 12.8 wt% and then decreases while further increasing the GDC content to 19.0 wt%. In Fig. 4i, current densities of the cell with the bare SFM cathode and the optimal 12.8 GDC–SFM cathode at 800 °C and various electrolysis voltages are compared. Stable current densities of 0.446, 0.263, 0.126 and 0.043 A cm^{-2} over a 12.8 GDC–SFM cathode were achieved at 1.6, 1.4, 1.2 and 1.0 V, respectively.

The electrochemical performance of a $(La_{0.6}Sr_{0.4})_{0.995}Co_{0.2}Fe_{0.8}O_{3-\delta}$ (LSCF) cathode in SOFCs was improved by Zhang *et al.*[71] *via* infiltration of $La_2NiO_{4+\delta}$ (LNO). It was found that a porous LSCF backbone coated with LNO nanoparticles is an attractive way to acquire a noticeable decrease in the polarization resistance and activation energy of the LSCF cathode, thus displaying high surface activity and enhanced oxygen transport properties. The LNO nanoparticles also led to a 67% increase in the peak power density and oper-

ation stability at 250 mA cm^{-2} with a low decay rate of 0.39% for about 500 h at 750 °C. The enhancement of ORR kinetics could be ascribed to the increase of the active surface area and active reaction regions from the heterostructured LSCF/LNO interface architecture, and/or favorable cation diffusion from LSCF to LNO.

Watchsman *et al.*[72] reported a high-performance surface modified $La_{0.6}Sr_{0.4}Co_{0.2}Fe_{0.8}O_{3-\delta}$-$Ce_{0.9}Gd_{0.1}O_{2-\delta}$ (LSCF–GDC) cathode for LT-SOFCs, prepared by solution infiltration. By carefully co-controlling the low calcination and operating temperature (<650 °C), the growth of infiltrated nanoparticles was obviously suppressed and the ORR was activated. In addition, these nanoelectrocatalysts remained highly active over 1300 h at 600 °C and exhibited exceptional stability under transient current loads – an essential feature for portable and automotive applications.

Using the infiltration process, Choi *et al.*[73] prepared a nanostructured $Sm_{0.5}Sr_{0.5}CoO_{3-\delta}$ (SSC) cathode functional layer (CFL) into porous $Gd_{0.2}Ce_{0.8}O_{2-\delta}$ (GDC). By controlling the drying process during the infiltration process, two distinct nanostructures of SSC, discrete coating and film-like coating, were prepared on the GDC scaffolds. The CFL with the film-like coating showed ~30% reduction in polarization resistance (R_p) and ~15% increase in the peak power density at 650 °C compared to the CFL with the discrete coating in spite of ~12-fold lower loading of infiltration materials.

Layered-structure cobaltite $PrBaCo_2O_{5+x}$ (PBC) nanoparticles were deposited into porous SDC backbones using an impregnation method.[74] The fabrication processing parameters of the composition of the precursor solution, PBC loading, and firing temperature have been studied to optimize the cathode microstructure and further to minimize the cathode interfacial polarization resistance, leading to a cathode interfacial polarization resistance of only 0.082 Ω cm^2 at 600 °C, much lower than those reported for the pure PBC electrode (0.86 Ω cm^2) and the PBC–SDC composite cathode (0.25 Ω cm^2). Both oxygen ion incorporation and charge transfer steps were greatly accelerated for the novel nanostructured PBC cathode, indicating that the impregnation process is very effective in fabricating a layered-structure cobaltite electrocatalyst for the IT-SOFC cathode with enhanced electrode performance. Similarly, Xi *et al.* impregnated $Sm_{0.5}Sr_{0.5}CoO_3$-δ (SSC) into $PrBaCo_2O_{5+\delta}$ (PBC) and obtained an ASR of 0.16 Ω cm^2 and a power density of 385 mW cm^{-2} at 700 °C.[75] Table 1 presents a performance comparison of the cells with various nanostructured cathodes.

In summary, surface modification through infiltration has played an increasingly important role in high-performance SOFCs. Although this method has been widely used in small lab-scale research, its implementation on a large scale is complicated considering two facts: (i) multiple cycles of impregnation and calcination are normally needed to accomplish sufficient conductivity and stability of the infiltrated electrodes, resulting in high time consumption and cost, and (ii) it is difficult to obtain a homogeneous distribution of the catalytic material manually dropwise over large areas.

Table 1 Performance comparison of the cells with various nanostructured cathodes

Cell configurations	Nanostructured cathode compositions	Sizes	Nanotechnologies	Cell performance (R_p, current densities, power densities and stability)	Ref.
GDC–LSCF/GDC/GDC–LSCF	1D $La_{0.8}Sr_{0.2}Co_{0.2}Fe_{0.8}O_{3-\delta}$ (LSCF)/$Ce_{0.8}Gd_{0.2}O_{1.9}$ (GDC) nanocomposite	—	Electrospinning, infiltration	0.10 Ω cm^2 at 650 °C	34
NiO-YSZ|YSZ|GDC|LSCF/GDC	LSCF nanofibers/20 wt% GDC	30 nm (GDC NPs)	Electrospinning, infiltration	1.07 W cm^{-2} at 750 °C	36
NiO-CGO/CGO/SSC nanofiber	SSC nanofiber	20–100 nm diameters	Electrospinning	0.010 Ω cm^2 at 700 °C, 1.09 W cm^{-2} at 700 °C	39
LSCF–GDC|LSGM|LSCF–GDC	ZrO_2 nanofilms@LSCF–GDC	10–15 nm (ZrO_2 films)	ALD deposition	Polarization ASR – 3 times lower, and exceptional stability for 4000 h at 700 °C	43
NiO-YSZ|NiO-YSZ AFL|YSZ|GDC interlayer|LSCF-DGC/LSC LSCF/GDC	LSCF–GDC nanocomposite film, nanoporous $La_{0.6}Sr_{0.4}CoO_{3-\delta}$	—	PLD deposition	0.030 Ω cm^2@0.75 V, ~2.2 and ~4.7 A cm^{-2} at 0.7 V at 650 °C and 700 °C	48
NiO-YSZ|YSZ|BSCF	BSCF nanofilm	40 nm	PLD deposition	1.12 W cm^{-2} at 800 °C	49
LnBCF|LSGM|LnBCF	CoO NPs@$Pr_{0.2}Ba_{0.8}Co_{0.7}Fe_{0.3}O_{3-\delta}$	20–100 nm	Exsolution	~0.119 Ω cm^2 at 550 °C	58
LSFN|YSZ|LFSN	NiFe NPs@LSFN	~20 nm	Exsolution	400 mW cm^{-2} in C_3H_8, 230 mW cm^{-2} in CH_4	61
NiO-YSZ|YSZ|GDC interlayer|LSCF–LNO	$La_2NiO_{4+\delta}$ NPs@LSCF	50 nm	Infiltration	0.042 Ω cm^2 at 700 °C, 697 mW cm^{-2} at 750 °C	71
PBC|SDC|PBC	$PrBaCo_2O_{5+x}$@SDC	50 nm	Infiltration	0.082 Ω cm^2 at 600 °C	74
NiO-BZCY|BZCY|PBC–SSC	$Sm_{0.5}Sr_{0.5}CoO_{3-\delta}$ NPs@PBC	—	Infiltration	0.16 Ω cm^2 at 700 °C, 385 mW cm^{-2} at 700 °C	75

To achieve fabricating large-area nanostructured cathodes, Dowd *et al.*[76] studied various parameters for infiltrating $La_{0.6}Sr_{0.4}CoO_{3-\delta}$ (LSCo) into the $La_{0.6}Sr_{0.4}Co_{0.2}Fe_{0.8}O_{3-\delta}$ (LSCF)–$Ce_{0.8}Sm_{0.2}O_2$ (SDC) cathode for a planar solid oxide fuel cell (SOFC) using an automated solution dispensing technique for industrial application of infiltrated SOFCs. Substrate temperature, chelating agent concentration, and surfactant type were explored to develop a one-step infiltration process for achieving an 8–10 wt% LSCo electrocatalyst in the cathode active layer.

3.5 Single atom-based cathode catalysts

Designing single-atom catalysts (SACs) by modulating catalytic sites at the atomic scale show high activity and minimize the use of metals, and SACs have unique selectivity that differs from nanoparticle catalysts owing to the lack of collection sites. The presence of high surface energies in the unsaturated and/or low-coordination active sites of SACs can lower the energy barrier and enhance charge transfer.[77,78]

SACs with a high ORR performance are mainly used in proton exchange membrane fuel cells (PEMFCs) and anion exchange membrane fuel cells (AEMFCs). However, few researchers have applied single-atom catalysts for SOFCs, mainly because the high operating temperature may lead to severe single-atom aggregation.[79] However, it is worth noting that reducible oxide supports, such as Fe_2O_3, CeO_2, TiO_2, *etc.*, are particularly suitable for stable single atoms due to strong covalent metal support interactions (CMSIs), and high-temperature thermally stable single-atom catalysts can be obtained through this interaction.[80] Li *et al.*[81] linked SACs with reversible proton-conducting solid oxide cells and selectively anchored Pt atoms to B sites in $Pr_4Ni_3O_{10+\delta}$. The obtained Pt single-atom catalyst could undergo a high temperature of 700 °C, and was highly active against oxygen reduction and oxygen evolution under 10% H_2O–air and 10% H_2O–10% CO_2–air conditions for 100 hours, respectively. They also assembled the Ni-BZCYYb1711|BZCYYb1711|Pt-$Pr_4Ni_3O_{10+\delta}$ cell; its electrochemical performance was improved by almost 100% compared with Ni-BZCYYb1711|BZCYYb1711| $Pr_4Ni_3O_{10+\delta}$. Importantly, this catalyst preparation method was suitable for industrial-scale production. Therefore, it is believed that single-atom cathode catalysts may be widely developed *via* the CMSI mechanism in the future.

The single-atom catalysts have potential for usage as cathodes in LT-SOFCs and IT-SOFCs owing to their highly catalytic activity. However, cost-effective large-scale production methods must be explored for wide applications in the future. The general impregnation–adsorption method has been reported by Hu *et al.* to construct platinum single-site catalysts by synergic micropore trapping and nitrogen anchoring on hierarchical nitrogen-doped carbon nanocages, which has also been extended to synthesize SACs of palladium, gold, iridium, *etc.*[82] In addition, the production of SAECs on a kilogram scale has been realized by a cost-effective mechanochemical approarch.[83] Finally, the introduction of a deep learning algorithm together with big data technology will greatly speed up the screening process and start up a new direction of rational design and modification for complicated SACs with the expected electrochemical catalytic performance.

3.6 Triple-conducting oxide cathodes

Proton-conducting SOFC systems have been found to be more appropriate for IT-SOFCs because of their lower activation energies and higher ionic conductivities at intermediate temperatures compared to oxygen ion-conducting SOFC systems.[84–87]

PLD has been used by Choi *et al.* to fabricate a thin dense layer of PBSCF between the porous PBSCF air electrode and the electrolyte.[88] The introduction of a dense PBSCF layer can significantly improve the contact and decrease ohmic resistance, leading to a remarkable electrolysis performance of 2 A cm^{-2}, at 1.3 V and 873 K.[89] As introduced before, the introduced nanoparticles or film on the surface of the air electrode of SOFCs can provide extra electrochemical reaction sites and pathways for the transfer of electrons and ions. Surface modification has been successfully applied to proton conducting SOFCs (H-SOFCs) for improving the performance of air electrodes.[90,91] It is reasonable to suggest that surface modification would be an efficient approach to improve the performance of air electrodes in H-SOECs, especially at low operating temperatures.

A basic requirement for the cathode material of high-performing proton conducting electrolyte-based SOFCs (H^+-SOFCs) is high conductivity and high chemical stability of electrons, oxide ions, and protons. In this regard, triple-conducting ($H^+/O^{2-}/e^-$) oxides (TCOs) are shown to be promising, having the ability to effectively extend electrochemically active sites from the interface between the cathode and the electrolyte to the entire surface of a cathode.[92–94]

A single-perovskite oxide SSC with high ORR activity was obtained by combining a common TCO material with SBC utilized to create a composite cathode for proton conducting electrolyte-based SOFCs.[92] Based on the performance of single cell NiO-$BaZr_{0.1}Ce_{0.7}Y_{0.1}Yb_{0.1}O_{3-\delta}$ (BCZYYb)‖BCZYYb‖SSC–SBC, the power density of the composite cathode SSC–SBC was found to be greatly enhanced in comparison with that of the SSC and SBC. Moreover, a much lower R_p was shown through electrochemical impedance spectroscopy (EIS) and a distribution in relaxation times (DRT) from the new composite cathode. Kim *et al.*[95] reported an excellent anode-supported H^+-SOFC with a TCO as a cathode material. Generally, mixed ionic (O^{2-}) and electronic conductors (MIECs) have been selected as the cathode material of H^+-SOFCs. In a H^+-SOFC system, however, MIEC cathodes limit the electrochemically active sites to the interface between the proton conducting electrolyte and the cathode. New approaches for the tailoring of cathode materials for H^+-SOFCs should therefore be considered. The electrochemical performance of NBSCF/BZCYYb/BZCYYb-NiO showed excellent long-term stability for 500 h at 1023 K with a high power density of 1.61 W cm^{-2}.

Recently, perovskite $PrNi_{0.5}Co_{0.5}O_{3-\delta}$ with TCO properties was developed as an oxygen electrode by Ding *et al.*[96] present-

ing a superior electrochemical performance at 400–600 °C. More importantly, the self-sustainable and reversible operation was successfully demonstrated by converting the generated hydrogen in the electrolysis mode to electricity without any hydrogen addition. The excellent electrocatalytic activity was attributed to the considerable proton conduction, as confirmed by the hydrogen permeation experiment, remarkable hydration behavior and computations.

It is found that when the oxygen electrode material of H^+-SOEC only has good electronic and oxygen ion conductivity characteristics, the reaction sites of the oxygen electrode are limited to the interface between the oxygen electrode material and the electrolyte, and the oxygen electrode has limited reaction active sites. However, when the oxygen electrode is a triple conductor for H^+, O^{2-} and electrons, the reaction active sites of the oxygen electrode can be extended to the entire electrode surface. Therefore, increasing the proton conductivity in the oxygen electrode rather than the oxygen ion conductivity is crucial for improving the performance of H^+-SOECs.

Based on a lot of data acquired from the published literature studies, the machine-learning (ML) method was introduced to accelerate the discovery of efficient mixed protonic–electronic conducting oxides. Ye *et al.*[97] screened and prepared $(La_{0.7}Ca_{0.3})(Co_{0.8}Ni_{0.2})O_3$ (LCCN 7382). The experimental results corresponded to the predicted results.

3.7 Cathodes of solid oxide electrolysis cells

Reversible solid oxide cells (RSOCs) can potentially address the seasonal energy storage challenge. When the residual electric energy is available, RSOCs operate in the electrolytic cell (EC) mode to convert H_2O and/or CO_2 into H_2 and/or CO as well as hydrocarbon fuels with a higher added value. During peak electricity usage periods or when additional electricity is needed to supplement energy, the reversible fuel cells can operate in the fuel cell (FC) mode to generate electricity. Since chemical fuels can be easily stored for a long time (or immediately used as renewable feedstock in a variety of industrial applications), RSOCs can alleviate the challenges of self-discharge and storage scaling cost challenges associated with batteries, and the conversion of renewable electric energy to chemical fuels forms a "electricity–hydrogen–electricity" hydrogen production, hydrogen storage and power generation system, and thus achieves a fully sustainable energy economy, as shown in Fig. 5.

In recent years, hydrogen production from electrolyzing water and carbon dioxide (CO_2) reduction *via* solid oxide electrolysis cell (SOECs) using renewable energies has attracted considerable attention due to its favorable thermodynamics and kinetics at high temperatures. A good steam electrode for SOECs should have sufficient pathways for both electron/proton and gas diffusion, as well as a high surface area for better catalytic reaction activity.[98,99] Therefore, both morphology and porosity of the electrode play key roles in the electrochemical performance in the electrode. Since the size of the water molecule (≈275 pm) is larger than that of the O_2 molecule (≈150 pm), the steam electrode in SOECs requires

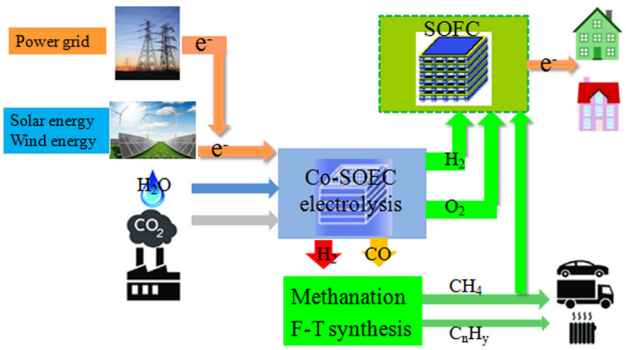

Fig. 5 Sustainable energy systems based on SOFC/SOEC technologies.

more porosity than the cathode in SOFCs for mass transfer. Consequently, the concept of a ultrahigh porous structure has been developed and proved to be effective to improve the electrode performance.[100] Taking an example, Chen *et al.*[101] reported a porous 3D fibrous cathode for IT-SOFCs with enhanced cell performance at 550 °C. The ORR was greatly enhanced by hollow fiber networks with high porosity and straight path for electrode reactions. In order to simplify the fabrication process and eliminate the use of high voltage, Dong *et al.*[102] developed a template-derived method to fabricate a highly porous, interwoven fibrous $Sm_{0.5}Sr_{0.5}CoO_3$ (SSC) cathode for SOFCs. The peak power density of the cell with the porous cathode was improved by 44.5 and 29.8% at 600 and 500 °C, respectively. It showed the effect of porosity in the fibrous electrode on electrode kinetics by enlarged TPBs and enhanced mass transfer. However, the fabrication processes of such a highly porous cathode were complicated, and it was challenging to incorporate them into the full cells with the structure integrity. In addition, its strength and flexibility are supposed to be poor, resulting in difficulty of mass production. Therefore, it is desired to develop highly porous nanostructured electrodes with adequate mass transfer pathways and sufficient mechanical strength in SOECs.[98,99]

The operating temperature of the cell with H-SOECs can be significantly reduced from beyond 800 to 600 °C or even lower due to its higher conductivity and lower activation energy. Wu *et al.*[99] reported a self-architectured ultraporous (SAUP) 3D steam electrode for efficient H-SOECs below 600 °C. As shown in Fig. 6, the electrolysis current density reached 2.02 A cm^{-2} at 1.6 V at 600 °C. In contrast to fast degradation in most O-SOECs, an enhanced performance was achieved during electrolysis at an applied voltage of 1.6 V at 500 °C for over 75 h, which was attributed to the "bridging" effect originating from reorganization of the steam electrode. The H-SOEC with the SAUP steam electrode is promising for next-generation steam electrolysis at reduced temperatures.

A double perovskite $Sr_2Fe_{1.3}Co_{0.2}Mo_{0.5}O_{6-\delta}$ (SFCM) with exsolved Co nanoparticles showed enhanced reaction activity and durability of SOECs for electrolysis of a H_2O, CO_2 or CO_2–H_2O mixture.[103] The Co nanoparticles were *in situ* exsolved

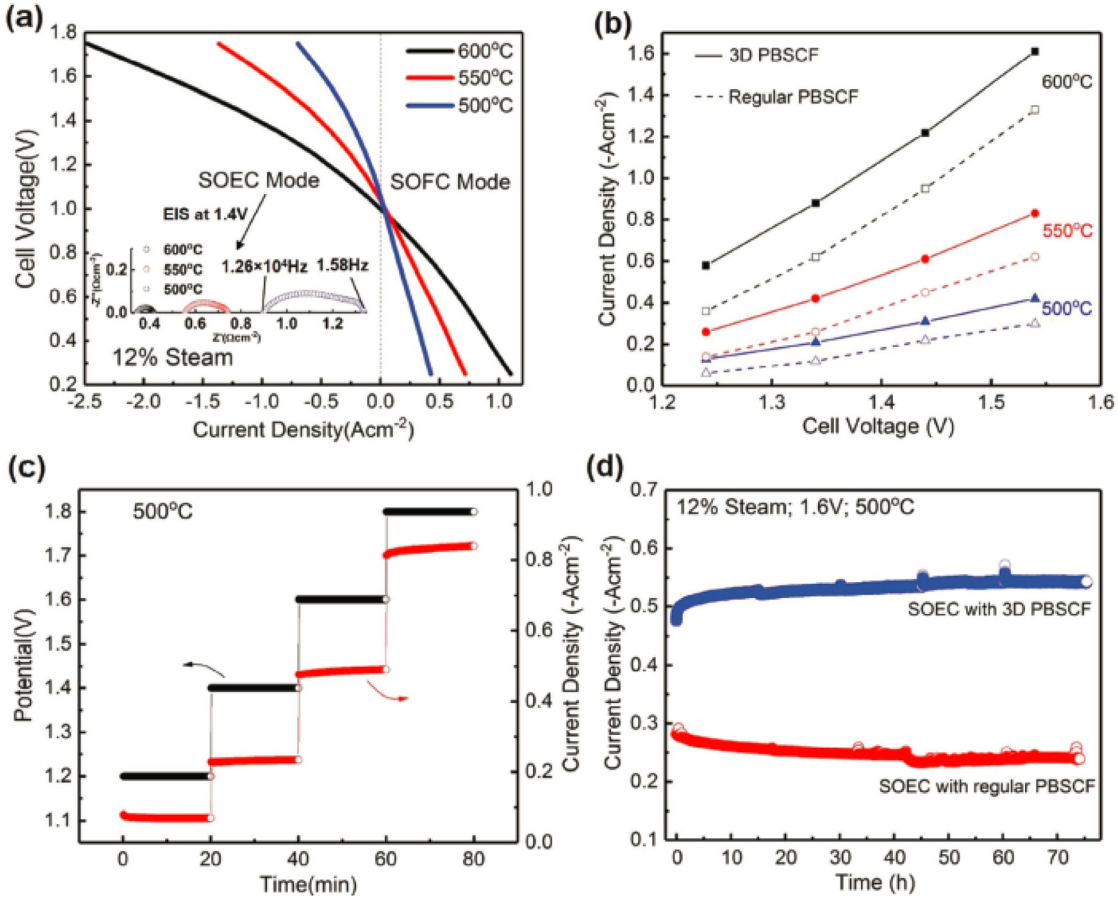

Fig. 6 (a) *I–V* curves of the solid oxide cell measured in the SOEC and SOFC modes at various temperatures; (b) electrolysis performance enhanced by a SAUP 3D PBSCF steam electrode when compared with that of the conventional PBSCF electrode at different temperatures; (c) short-term electrolysis at different applied voltages at 500 °C and (d) durability of SOECs with a 3D PBSCF steam electrode (blue) and a conventional PBSCF steam electrode (red) under an applied voltage of 1.6 V at 500 °C. (d) The performance of SOECs with conventional PBSCF degrades with time, while that of SOECs with 3D PBSCF shows constant activation, reprinted from ref. 99 with permission from Wiley-VCH Verlag GmbH & Co. KGaA.

from the parental SFCM in 10% H_2–90% N_2 and they could remain stable under an atmosphere of 50% CO_2–50% H_2 or 50% CO_2–50% CO. The cells of SFCM‖$La_{0.8}Sr_{0.2}Ga_{0.83}Mg_{0.17}O_{3-\delta}$ (LSGM)‖SFCM showed excellent electrochemical performances in the electrolysis mode, with a low polarization resistance of 0.24 Ω cm^2 in 50% H_2O–50% H_2 at an open-circuit voltage. The resistances of the cell can be significantly decreased by the *in situ* exsolved Co nanoparticles from the SFCM electrode, thus leading to higher activity and better stability.

Fe-exsolved ceria was found to be highly efficient as a SOEC cathode for CO_2 electrolysis.[104] Dopant Fe is partially reduced under working conditions, forming dispersed Fe^0 nanoparticles, which remarkably enhances the catalytic activity for the CO_2 reduction reaction. At 700 °C, the cathode polarization resistance reached 0.57 Ω cm^2, and the chemical surface exchange coefficient for CO_2 reduction was 1.68×10^{-3} cm s^{-1}, showing a better performance than metal-exsolved perovskite cathodes at 800 °C.

Layered-perovskite oxide electrodes with *in situ* exsolved Co–Fe alloy nanoparticles were developed for efficient CO_2 electrolysis to produce carbon monoxide (CO).[105] Using a double perovskite oxide $Sr_2Ti_{0.8}Co_{0.2}FeO_{6-\delta}$ as a solid precursor, a Ruddlesden–Popper phase oxide matrix with exsolved Co–Fe alloy nanoparticles uniformly distributed on the surface (Co–Fe–STCF) was synthesized by thermal reduction. The cell with a mixture of Co–Fe–STCF and $Sm_{0.2}Ce_{0.8}O_{2-\delta}$ (SDC) as the fuel electrode exhibited an outstanding performance for CO_2 electrolysis, with a polarization resistance (R_p) as low as 0.22 Ω cm^2 at 800 °C. A current density of 1.26 A cm^{-2} was achieved at a bias of 1.6 V at 800 °C, and the CO production rate reached 8.75 mL min^{-1} cm^{-2} with a high value of Faraday efficiency (~100%).

$Sr_2Fe_{1.5}Mo_{0.5}O_{6-\delta}$ (SFM) is one kind of promising cathode material for SOECs, but suffers from insufficient activity for the CO_2 reduction reaction (CO_2RR). GDC nanoparticles were infiltrated onto the SFM surface to construct a composite GDC–SFM cathode and improve the CO_2RR performance in SOECs.[70] Temperature-programmed desorption of CO_2 measurements suggests that the infiltration of GDC nanoparticles significantly increases the density of surface active sites and TPBs, which are beneficial for CO_2 adsorption and

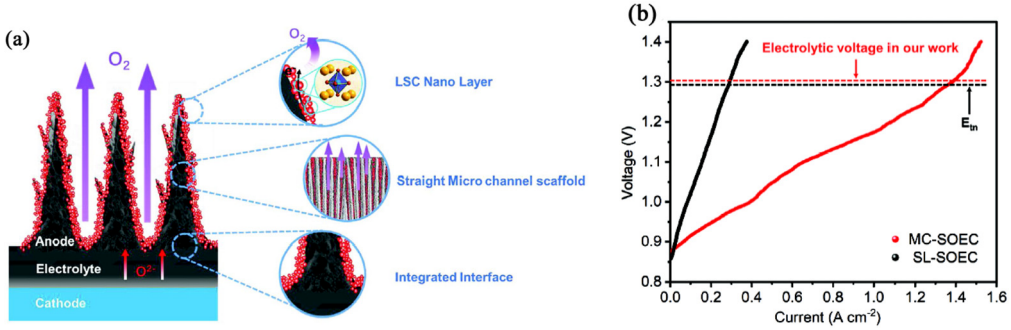

Fig. 7 (a) A schematic illustration of the novel SOEC with a nano/micro-channel air electrode and (b) *I*–*V* curve of the MC-SOEC and SL-SOEC in the electrolysis mode at 800 °C, reprinted from ref. 106 with permission from Wiley-VCH Verlag GmbH & Co. KGaA.

subsequent conversion. EIS results indicate that the polarization resistance of the 12.8 wt% GDC–SFM cathode was obviously decreased from 0.46 to 0.30 Ω cm^2 after the infiltration of GDC nanoparticles.

To extend the TPBs, Cao *et al.*[106] prepared a unique SOEC with a vertically aligned micro-scale channel air electrode scaffold, as shown in Fig. 7a. This unique structure enhanced interfacial adherence ability, facilitated oxygen generation stability and accelerated oxygen release. A SOEC with this micro-/nano channel (MC) structure achieved a 4.8 times higher current density of 1.38 A cm^{-2} at 1.3 V, compared with that of the sponge-like (SL)-SOEC (0.29 A cm^{-2}) (Fig. 7b). However, the testing temperature was still higher at 800 °C and the long-term stability was a concern.

SOECs is a kind of efficient apparatus for hydrogen production from electrolyzing water as well as co-electrolyzing water and CO_2 utilizing renewable energies, such as wind energy, solar energy and other clean energies, which may play a key role in adjusting peaks of electric grids and achieving carbon neutralization. However, high-performance cathode materials operating at low and intermediate temperatures are still desired.

3.8 Computational design, machine learning (ML) and artificial intelligence (AI)

Data-intensive machine learning (ML) techniques have been widely used in materials science.[107] For example, the determination of $H^+/O^{2-}/e^-$ conductivities of TCOs is difficult. However, ML techniques can be utilized to address this challenge. ML models can be trained according to the reported experimental database, which can be used to predict the conductivities of TCOs for various compositions, structures, and operating conditions. The conductivities of 97 625 perovskite oxides were efficiently predicted by constructing an XG-Boost model under different conditions in wet H_2 and air. So, the researcher can gain insight into the factors that determine conductivity, which is instructive for material design and optimization.[107,108]

Recently, a machine-learning technique was applied to the development of a highly active fuel cell cathode by Ni *et al.*[109] They demonstrated an experimentally validated machine-learning-driven approach for accelerating the discovery of efficient oxygen reduction electrodes, where the ionic Lewis acid strength (ISA) was introduced as an effective physical descriptor for the oxygen reduction reaction activity of perovskite oxides.

In addition, ML could also expedite the discovery of durable cathode materials.[107–110] Cathode materials undergo various degradation reactions, such as phase transformations, chemical reactions with the electrolyte, mismatch of the thermal expansion coefficient with the electrolyte, or structural changes, which can lead to a loss of catalytic activity, an increase in R_p, and reduced oxygen surface exchange kinetics. These detrimental effects can severely impact the overall performance and efficiency of the cell. To achieve high durability of cathode materials, there is an urgent need to develop advanced technologies including ML to promote the discovery of durable cathode materials.

Artificial intelligence (AI) has been used to create theoretical SOFC models to minimize the time necessary to identify the operational optimum over a wide range of parameters as well as the total cost of the system. Afroze *et al.* reviewed the function of AI in improving SOFC performance.[111] It is noted that machine learning methods were also used to simulate the performance of solid oxide electrolyzers.[112] The significant roles of AI are becoming increasingly evident in the nanoengineering of electrodes for SOCs, particularly helpful for nanomaterial research and development.

AI technique has also been used to analyze the performance of the anode and cathode electrodes of SOFCs under various key parameters that normally influence the efficiency of the electrodes. Computational trials with the aid of AI would not only reduce the preparation cost, but also ensure less time consumption. Among the various AI methods available in the literature, the Support Vector Machine (SVM) is believed to be one of the excellent and effective machine learning techniques. Subramanian *et al.* developed a SVM model and predicted the maximum current density and power density of the cell with a NiO–SDC composite anode and a $La_{0.6}Sr_{0.4}Co_{0.2}Fe_{0.8}O_{3-\delta}$ (LSCF) cathode.[113] To validate the results as predicted from SVM, they prepared a YSZ electrolyte-supported single cell with a NiO–SDC anode and a LSCF

cathode. It was found that that the theoretically predicted data current and power densities of the electrodes from the SVM approach agree well with the experimental results.

4. Summary and outlook

Solid oxide fuel cells (SOFCs) operating at low and intermediate temperatures are gaining considerable attention for applications in energy conversion, chemical synthesis and electrolysis due to their potential long-term stability and economic competitiveness for a large number of applications. However, large ohmic and polarization losses reduce the cell performance. The ohmic and polarization losses are mainly due to oxygen ion or proton transport through the electrolyte and the sluggish reaction kinetics on the surfaces of the electrodes, respectively. The approaches for reducing such losses include using electrolyte materials with fast ionic conductivity at low temperatures, reducing electrolyte thickness, increasing the reactant concentration and the number of possible reaction sites and decreasing the activation barrier. The cathode microstructure has been improved by optimizing the connectivity and size distribution between particles of each solid phase to yield a larger TPB that is accessible for oxygen reduction.

By using mixed ionic electronic conductors (MIECs), such as perovskite $La_{0.6}Sr_{0.4}CoO_{3-\delta}$ (LSC), $La_{0.6}Sr_{0.4}Co_{0.2}Fe_{0.8}O_{3-\delta}$ (LSCF), and $Sm_{0.5}Sr_{0.5}CoO_{3-\delta}$ (SSC), the ORR kinetics can be significantly enhanced due to their relatively high ionic and electronic conductivities and fast oxygen exchange. However, the polarization resistance of the cathode still dominates the overall cell performance at low and intermediate temperatures. Modulating material properties *via* an effective nanoengineering approach can largely boost the electrochemical performance of cathodes for the development of next-generation SOFCs operating at low and intermediate temperatures.

Nanostructured composite electrodes made by a carefully conducted infiltration process are some of the most promising electrode structures for LT-SOFCs and IT-SOFCs, due to their ability to enlarge TPBs and thus promote the ORR properties. However, the deposited particles are prone to coarsening during high temperature operation. In addition, to reveal the fundamental science during the impregnation itself, a systematic investigation on the process of wetting and chemical interactions during operation and an in-depth understanding of the engineering of this technique for electrode modification are highly desirable. For industrial applications, the infiltration process should be optimized, and made simple and cost-effective.

In situ exsolution nanoparticles from perovskite materials can have good control over the size and distribution of the exsolved particles by adjusting the temperature and time under a reducing atmosphere. Therefore, the exsolved nanoparticles show excellent resistance to coarsening. However, for the cathode material under an oxidizing atmosphere, the exsolved metal nanoparticles are easily reoxidized and dissolved back into the perovskite lattice. The negative voltage driven strategy may provide a new approach for designing high-performance cathode catalysts for next-generation SOFCs.

Furthermore, the presence of high surface energies in the unsaturated and/or low-coordination active sites of SACs can lower the energy barrier and enhance charge transfer. Therefore, single-atom based cathode catalysts will undoubtedly have wide applications in the future. However, from the industrial standpoint, the catalyst synthesis method on a large scale is still challenging.

To further reduce the polarization resistance of the cathode, adding a cathode functional layer (CFL) has been proved as an effective strategy for enhancing electrocatalytic activity through extending TPBs. In addition, for H^+-SOFCs, the triple conducting oxides as cathodes can effectively extend the electrochemically active sites from the interface between the cathode and the electrolyte to the entire surface of the cathode.

In summary, nanoengineering of electrodes employed for SOFCs has emerged as a versatile tool for significantly enhancing the electrochemical performance of next-generation SOFCs operating at low and intermediate temperatures, but there are still some challenges for integrating it into practical cells suitable for widespread application, such as the development of scalable and cost-effective approaches, inhibition of the coarsening of the nanoparticles and single-atom based catalysts at high temperatures, unlocking the quantitative correlation among TPBs, interfacial polarization resistance, the catalytic activity of the cathodes, *etc*. The combination of computational design, machine learning (ML) and artificial intelligence (AI) provides a revolutionary approach to achieve this purpose. AI can possibly contribute in unveiling complex relationships between the microstructure of the cathodes and their activity.

In the future, the study on SOFCs should focus on the development of cost-effective new materials, processes and concepts for next-generation SOFCs operating at lower temperatures (<600 °C) with hydrogen or hydrocarbon as fuel as well as high-performance reversible solid oxide cells (RSOCs) for seasonal energy storage, which may play a pivotal role in achieving carbon neutralization.

All the nanoengineering techniques discussed in this review may be utilized in fabricating electrode materials for other electrochemical energy conversion and storage devices, like the emerging solid-state batteries.

Data availability

All data are available upon request.

Conflicts of interest

There are no conflicts to declare.

Acknowledgements

The authors acknowledge the financial support from the National Key R&D Program of China (No. 2023YFE0115800) and the National Natural Science Foundation of China (No. 52472271).

References

1 C. W. Sun and U. Stimming, Recent anode advances in solid oxide fuel cells, *J. Power Sources*, 2007, **171**, 247–260.
2 C. W. Sun, R. Hui and J. Roller, Cathode materials for solid oxide fuel cells: A review, *J. Solid State Electrochem.*, 2010, **14**, 1125–1144.
3 B. C. H. Steel and A. Heinzel, Materials for fuel-cell technologies, *Nature*, 2001, **414**, 345–352.
4 C. W. Sun and U. Stimming, Synthesis and characterization of NH_4PO_3 based composite with superior proton conductivity for intermediate temperature fuel cells, *Electrochim. Acta*, 2008, **53**, 6417–6422.
5 C. W. Sun, Z. Xie, C. R. Xia, H. Li and L. Q. Chen, Investigations of mesoporous CeO_2-Ru as a reforming catalyst layer for solid oxide fuel cells, *Electrochem. Commun.*, 2006, **8**, 833–838.
6 Q. Yang, J. Chen, C. W. Sun and L. Q. Chen, Direct Operation of methane fueled solid oxide fuel cells with Ni cermet anode via Sn modification, *Int. J. Hydrogen Energy*, 2016, **41**, 11391–11398.
7 Q. Yang, F. T. Chai, C. Ma, C. W. Sun, S. Q. Shi and L. Q. Chen, Enhanced coking tolerance of MgO-promoted Ni cermet anode for hydrocarbon fueled solid oxide fuel cells, *J. Mater. Chem. A*, 2016, **4**, 18031–18036.
8 C. W. Sun, C. L. López and J. A. Alonso, Elucidating the diffusion pathway of protons in ammonium polyphosphate: a potential electrolyte for intermediate temperature fuel cells, *J. Mater. Chem. A*, 2017, **5**, 7839–7844.
9 C. W. Sun, L. L. Chen, S. Q. Shi, B. Reeb, C. A. López, J. A. Alonso and U. Stimming, Visualization of the diffusion pathway of protons in the ammonium polyphosphate for intermediate temperature fuel cells, *Inorg. Chem.*, 2018, **57**, 676–680.
10 W. Zhang, F. S. Yin, Z. H. Cheng, S. P. Peng and C. W. Sun, Heterogeneous MgO-modified Ni_3Sn cermet anode for hydrocarbon-fueled solid oxide fuel cells, *Fuel*, 2023, **354**, 129356.
11 J. G. Lee, J. H. Park and Y. G. Shul, Tailoring gadolinium-doped ceria-based solid oxide fuel cells to achieve 2 W cm^{-2} at 550 °C, *Nat. Commun.*, 2014, **5**, 4045.
12 Y. L. Huang, A. M. Hussain and E. D. Watchsman, Nanoscale cathode modification for high performance and stable low-temperature solid oxide fuel cells (SOFCs), *Nano Energy*, 2018, **49**, 186–192.
13 M. R. Li, M. W. Zhao, F. Li, W. Zhou, V. K. Peterson, X. Y. Xu, Z. P. Shao, I. Gentle and Z. H. Zhu, A niobium and tantalum co-doped perovskite cathode for solid oxide fuel cells operating below 500 °C, *Nat. Commun.*, 2017, **8**, 13990.
14 R. J. Gorte and J. M. Vohs, Novel SOFC anodes for the direct electrochemical oxidation of hydrocarbons, *J. Catal.*, 2003, **216**, 477–486.
15 S. B. Alder, Factors governing oxygen reduction in solid oxide fuel cell cathodes, *Chem. Rev.*, 2004, **104**, 4791–4844.
16 L. Antoni, Materials for solid oxide fuel cells: the challenge of their stability, *Mater. Sci. Forum*, 2004, **461–464**, 1073–1090.
17 T. Tsai and S. A. Barnett, Effect of LSM-YSZ cathode on thin-electrolyte solid oxide fuel cell performance, *Solid State Ionics*, 1997, **93**, 207–217.
18 T. P. Holme, R. Pornprasertsuk and F. B. Prinz, Interpretation of low temperature solid oxide fuel cell electrochemical impedance spectra, *J. Electrochem. Soc.*, 2010, **157**, B64–B70.
19 E. Siebert, A. Hammouche and M. Kleitz, Impedance spectroscopy analysis of $La_{1(-x}Sr_xMnO_3$-yttria-stabilized zirconia electrode kinetics, *Electrochim. Acta*, 1995, **40**, 1741–1753.
20 M. J. Jørgensen and M. Mogensen, Impedance of solid oxide fuel cell LSM/YSZ composite cathodes, *J. Electrochem. Soc.*, 2001, **148**, A433–A442.
21 F. S. Baumann, J. Fleig, H. U. Habermeier and J. Maier, Impedance spectroscopic study on well-defined (La,Sr)(Co,Fe)$O_{3-(}$ model electrodes, *Solid State Ionics*, 2006, **177**, 1071–1081.
22 J. M. Serra, V. B. Vert, M. Betz, V. A. C. Haanappel, W. A. Meulenberg and F. Tiet, Screening of A-substitution in the system $A_{0.68}Sr_{0.3}Fe_{0.8}Co_{0.2}O_{3-(}$ for SOFC cathodes, *J. Electrochem. Soc.*, 2008, **155**, B207–B214.
23 J. Fleig, Solid oxide fuel cell cathodes: polarization mechanisms and modeling of the electrochemical performance, *Annu. Rev. Mater. Res.*, 2003, **33**, 361–382.
24 K. Eguchi, T. Setoguchi, T. Inoue and H. Arai, Electrical properties of ceria-based oxides and their application to solid oxide fuel cells, *Solid State Ionics*, 1992, **52**, 165–172.
25 T. Ishihara, H. Matsuda and Y. Takita, Doped $LaGaO_3$ perovskite type oxide as a new oxide ionic conductor, *J. Am. Chem. Soc.*, 1994, **116**, 3801–3803.
26 K. Huang, M. Feng, J. B. Goodenough and C. Milliken, Electrode performance test on single ceramic fuel cells using as electrolyte Sr- and Mg-doped $LaGaO_3$, *J. Electrochem. Soc.*, 1997, **144**, 3620–3624.
27 S. B. Adler, J. A. Lane and B. C. H. Steele, Electrode kinetics of porous mixed-conducting oxygen electrodes, *J. Electrochem. Soc.*, 1996, **143**, 3554–3564.
28 B. C. H. Steele, K. M. Hori and S. Uchino, Kinetic parameters influencing the performance of IT-SOFC composite electrodes, *Solid State Ionics*, 2000, **135**, 445–450.
29 C. W. Sun, J. A. Alonso and J. J. Bian, Recent Advances in Perovskite-type Oxides for Energy Conversion and Storage Applications, *Adv. Energy Mater.*, 2020, **10**, 202000459.

30 W. Yang, H. R. Zhang, C. W. Sun, L. L. Liu, J. A. Alonso, M. T. Fernández-Díaz and L. Q. Chen, Insight into the structure and functional application of $Sr_{0.95}Ce_{0.05}CoO_{3-(}$ cathode for solid oxide fuel cells, *Inorg. Chem.*, 2015, **54**, 3477–3485.

31 Y. D. Gong, C. W. Sun, Q. A. Huang, J. A. Alonso, M. T. Fernández-Díaz and L. Q. Chen, Dynamic octahedral breathing in oxygen-deficient $Ba_{0.9}Co_{0.7}Fe_{0.2}Nb_{0.1}O_{3-\delta}$ perovskite performing as a cathode for intermediate-temperature solid oxide fuel cells, *Inorg. Chem.*, 2016, **55**, 3091–3097.

32 W. Yang, T. Hong, S. Li, Z. H. Ma, C. W. Sun, C. R. Xia and L. Q. Chen, Perovskite $Sr_{1(-x}Ce_xCoO_{3-\delta}$ ($0.05 \leq x \leq 0.15$) as Cathodes for Intermediate Temperature Solid Oxide Fuel Cells, *ACS Appl. Mater. Interfaces*, 2013, **5**, 1143–1148.

33 M. G. Bellino, J. G. Sacancell, D. G. Lamas, A. G. Leyva and N. E. W. Reca, High-performance solid-oxide fuel cell cathodes based on cobaltite nanotubes, *J. Am. Chem. Soc.*, 2007, **129**, 3066–3067.

34 E. Q. Zhao, Z. Jia, L. Zhao, Y. P. Xiong, C. W. Sun and M. E. Brito, One dimensional $La_{0.8}Sr_{0.2}Co_{0.2}Fe_{0.8}O_{3-(}$/$Ce_{0.8}Gd_{0.2}O_{1.9}$ nanocomposite cathodes for intermediate temperature solid oxide fuel cells, *J. Power Sources*, 2012, **219**, 133–139.

35 Z. Liu, Y. Gu and L. Bi, Applications of electrospun nanofibers in solid oxide fuel cells- a review, *J. Alloys Compd.*, 2023, **937**, 168288.

36 M. J. Zhi, S. W. Lee, N. Miller, N. H. Menzler and N. Q. Wu, An intermediate-temperature solid oxide fuel cell with electrospun nanofiber cathode, *Energy Environ. Sci.*, 2012, **5**, 7066–7071.

37 J. Parbey, M. Xu, J. L. Lei, M. Espinoza-Andaluz, T. S. Li and M. Andersson, Electrospun fabrication of nanofibers as high-performance cathodes of solid oxide fuel cells, *Ceram. Int.*, 2020, **46**, 6969–6972.

38 C. R. Xia, W. Rauch, F. L. Chen and M. L. Liu, $Sm_{0.5}Sr_{0.5}CoO_3$ cathodes for low-temperature SOFCs, *Solid State Ionics*, 2002, **149**, 11–19.

39 C. L. Chang, C. S. Hsu, J. B. Huang, P. H. Hsu and B. H. Hwang, Preparation and characterization of SOFC cathodes made of SSC nanofibers, *J. Alloys Compd.*, 2015, **620**, 233–239.

40 M. G. Bellino, J. G. Sacancell, D. G. Lamas, A. G. Leyva and N. E. W. Reca, High-performance solid-oxide fuel cell cathodes based on cobaltite nanotubes, *J. Am. Chem. Soc.*, 2007, **129**, 3066–3067.

41 J. Sacanell, A. G. Leyva, M. G. Bellino and D. G. Lamas, Nanotubes of rare earth cobalt oxides for cathodes of intermediate-temperature solid oxide fuel cells, *J. Power Sources*, 2010, **195**, 1786–1792.

42 A. S. Asundi, J. A. Raiford and S. F. Bent, Opportunities for atomic layer deposition in emerging energy technologies, *ACS Energy Lett.*, 2019, **4**, 908–925.

43 Y. H. Gong, R. L. Patel, X. H. Liang, D. Palacio, X. Y. Song, J. B. Goodenough and K. Huang, Atomic layer deposition functionalized composite SOFC cathode $La_{0.6}Sr_{0.4}Fe_{0.8}Co_{0.2}O_{3-(}$-$Gd_{0.2}Ce_{0.8}O_{1.9}$: enhanced long-term stability, *Chem. Mater.*, 2013, **25**, 4224–4231.

44 Y. H. Gong, D. Palacio, X. Y. Song, R. L. Patel, X. H. Liang, J. B. Goodenough and K. Huang, Stabilizing nanostructured solid oxide fuel cell cathode with atomic layer deposition, *Nano Lett.*, 2013, **13**, 4340–4345.

45 O. Celikbilek, C. A. Thieu, F. Agnese, E. Cali, C. Lenser, N. H. Menzler, J. W. Son, S. J. Skinner and E. Djurado, Enhanced catalytic activity of nanostructured, A-site deficient $(La_{0.7}Sr_{0.3})_{0.95}(Co_{0.2}Fe_{0.8})O_{3-(}$ for SOFC cathodes, *J. Mater. Chem. A*, 2019, **7**, 25102–25111.

46 J. Januschewsky, M. Ahrens, A. Opitz, F. Kubel and J. Fleig, Optimized $La_{0.6}Sr_{0.4}CoO_{3-(}$ thin-film electrodes with extremely fast oxygen-reduction kinetics, *Adv. Funct. Mater.*, 2009, **19**, 3151–3156.

47 K. Develos-Bagarinao, R. A. Budiman, T. Ishiyama, K. Yamaji and H. Kishimoto, Leveraging catalytic effects of heterointerfaces through multilayering for superior cathode performance, *J. Power Sources*, 2020, **480**, 229094.

48 K. Develos-Bagarinao, T. Ishiyama, H. Kishimoto, H. Shimada and K. Yamaji, Nanoengineering of cathode layers for solid oxide fuel cells to achieve superior power densities, *Nat. Commun.*, 2021, **12**, 3979.

49 B. Liu, X. B. Chen, Y. L. Dong, S. S. Mao and M. J. Cheng, A high-performance, nanostructured $Ba_{0.5}Sr_{0.5}Co_{0.8}Fe_{0.2}O_{3-(}$ cathode for solid-oxide fuel cells, *Adv. Energy Mater.*, 2001, **1**, 343–346.

50 W. Zhang, H. Wang, K. Guan, J. Meng, Z. Wei, X. Liu and J. Meng, Enhanced anode performance and coking resistance by in situ exsolved multiple-twinned Co-Fe nanoparticles for solid oxide fuel cells, *ACS Appl. Mater. Interfaces*, 2020, **12**, 461–473.

51 M. Chen, B. H. Kim, Q. Xu, B. G. Ahn and D. P. Huang, Fabrication and performance of anode-supported solid oxide fuel cells via slurry spin coating, *J. Membr. Sci.*, 2010, **360**, 461–468.

52 T. V. Gestel, D. Sebold, H. P. Buchkremer and D. Stöver, Assembly of 8YSZ nanoparticles into gas-tight 1-2 μm thick 8YSZ electrolyte layers using wet coating methods, *J. Eur. Ceram. Soc.*, 2012, **32**, 9–26.

53 J. G. Lee, J. H. Park and Y. G. Shul, Tailoring gadolinium-doped ceria-based solid oxide fuel cells to achieve 2 W cm^{-2} at 550 °C, *Nat. Commun.*, 2014, **5**, 4045.

54 J. Leng, Z. Wang, J. Wang, H. H. Wu, G. Yan, X. Li, H. Guo, Y. Liu, Q. Zhang and Z. Guo, Advances in nanostructures fabricated via spray pyrolysis and their applications in energy storage and conversion, *Chem. Soc. Rev.*, 2019, **48**, 3015–3072.

55 K. Kousi, C. Tang, I. S. Metcalfe and D. Neagu, Emergence and future of exsolved materials, *Small*, 2021, **17**, 2006479.

56 J. H. Kim, J. K. Kim, J. Liu, A. Curcio, J. S. Jang, I. D. Kim, F. Ciucci and W. Jung, Nanoparticle ex-solution for supported catalysts: materials design, mechanism and future perspectives, *ACS Nano*, 2021, **15**, 81–110.

57 J. H. Myung, D. Neagu, D. N. Miller and J. T. S. Irvine, Switching on electrocatalytic activity in solid oxide cells, *Nature*, 2016, **537**, 528–531.

58 W. W. Zhang, H. C. Wang, X. P. Chen, X. J. Liu and J. Meng, Manipulation of rare earth on voltage-driven *in situ* exsolution process of perovskite cathodes for low-temperature solid oxide fuel cells, *Chem. Eng. J.*, 2022, **446**, 136934.

59 R. Zhou, Y. Y. Gu, H. L. Dai, Y. S. Xu and L. Bi, *In situ* exsolution of $PrO_{2(-x}$ nanoparticles boost the performance of transitional $Pr_{0.5}Sr_{0.5}MnO_{3-(}$ cathode for proton-conducting solid oxide fuel cells, *J. Eur. Ceram. Soc.*, 2023, **43**, 6612–6621.

60 Q. Liu, X. Dong, G. Xiao, F. Zhao and F. L. Chen, A novel electrode material for symmetrical SOFCs, *Adv. Mater.*, 2010, **22**, 5478–5482.

61 Z. H. Ma, C. W. Sun, C. Ma, H. Wu, Z. L. Zhan and L. Q. Chen, A highly active Ni-doped $La_{0.6}Sr_{0.4}FeO_{3-(}$ symmetrical electrode for hydrocarbon-fueled solid oxide fuel cells, *Chin. J. Catal.*, 2016, **37**, 1347–1353.

62 S. P. Jiang, Nanoscale and nano-structured electrodes of solid oxide fuel cells by infiltration: advances and challenges, *Int. J. Hydrogen Energy*, 2012, **37**, 449–470.

63 D. Ding, A. Li, S. Y. Lai, K. Gerdes and M. L. Liu, Enhancing SOFC cathode performance by surface modification through infiltration, *Energy Environ. Sci.*, 2014, **7**, 552–575.

64 J. M. Vohs and R. J. Gorte, High-performance SOFC cathodes prepared by infiltration, *Adv. Mater.*, 2009, **21**, 943–956.

65 F. L. Liang, J. Chen, J. L. Cheng, S. P. Jiang, T. M. He, J. Pu and J. Li, Novel nano-structured Pd plus yttrium doped ZrO_2 cathodes for intermediate temperature solid oxide fuel cells, *Electrochem. Commun.*, 2008, **10**, 42–46.

66 Y. Y. Huang, J. M. Vohs and R. J. Gorte, Fabrication of Sr-doped $LaFeO_3$-YSZ composite cathodes, *J. Electrochem. Soc.*, 2004, **151**, A646–A651.

67 C. Yuan, T. Luo, J. L. Li, X. Meng, J. Q. Qian, X. F. Ye, Z. L. Zhan, C. R. Xia and S. R. Wang, Infiltrated porous YSZ as a cathode active layer for cathode-supported solid oxide fuel cells, *Electrochem. Commun.*, 2014, **46**, 40–43.

68 T. Z. Sholklapper, C. Lu, C. P. Jacobson, S. J. Visco and L. C. De Jonghe, LSM-infiltrated solid oxide fuel cell cathodes, *Electrochem. Solid-State Lett.*, 2006, **9**, A376–A378.

69 T. Z. Sholklapper, H. Kurokawa, C. P. Jacobson, S. J. Visco and L. C. De Jonghe, Nanostructured solid oxide fuel cell electrodes, *Nano Lett.*, 2007, **7**, 2136–2141.

70 H. F. Lv, Y. J. Zhou, X. M. Zhang, Y. F. Song, Q. X. Liu, G. X. Wang and X. H. Bao, Infiltration of $Ce_{0.8}Gd_{0.2}O_{1.9}$ nanoparticles on $Sr_2Fe_{1.5}Mo_{0.5}O_{6-(}$ cathode for CO_2 electroreduction in solid oxide electrolysis cell, *J. Energy Chem.*, 2019, **35**, 71–78.

71 X. X. Zhang, H. Zhang and X. B. Liu, High performance $La_2NiO_{4+(}$-infiltrated $(La_{0.6}Sr_{0.4})_{0.995}Co_{0.2}Fe_{0.8}O_{3-(}$ cathode for solid oxide fuel cells, *J. Power Sources*, 2014, **269**, 412–417.

72 Y. L. Huang, A. M. Hussain and E. D. Watchsman, Nanoscale cathode modification for high performance and stable low-temperature solid oxide fuel cells (SOFCs), *Nano Energy*, 2018, **49**, 186–192.

73 M. Choi, J. Lee and W. Lee, Nano-film coated cathode functional layers towards high performance solid oxide fuel cells, *J. Mater. Chem. A*, 2018, **6**, 11811–11818.

74 Y. Wang, H. Zhang, F. L. Chen and C. R. Xia, Electrochemical characteristics of nano-structured $PrBaCo_2O_{5+x}$ cathodes fabricated with ion impregnation process, *J. Power Sources*, 2012, **203**, 34–41.

75 X. Xi, X. Chen, G. Hou, N. Xu, Q. Zhang and Z. Tao, Fabrication and evaluation of $Sm_{0.5}Sr_{0.5}CoO_{3-\delta}$ impregnated $PrBaCo_2O_{5+\delta}$ composite cathode for proton conducting SOFCs, *Ceram. Int.*, 2014, **40**, 13753–13756.

76 R. P. Dowd Jr., S. W. Lee, Y. Y. Fan and K. Gerdes, Engineering the solid oxide fuel cell electrocatalyst infiltration technique for industrial use, *Int. J. Hydrogen Energy*, 2016, **41**, 14971–14981.

77 R. Lang, T. Li, D. Matsumura, S. Miao, Y. Ren, Y. T. Cui, Y. Tan, B. Qiao, L. Li, A. Wang, X. Wang and T. Zhang, Hydroformylation of olefins by a rhodium single-atom catalyst with activity comparable to $RhCl(PPh_3)_3$, *Angew. Chem., Int. Ed.*, 2016, **55**, 16054–16058.

78 Y. Pan, S. Liu, K. Sun, X. Chen, B. Wang, K. Wu, X. Cao, W. C. Cheong, R. Shen, A. Han, Z. Chen, L. Zheng, J. Luo, Y. Lin, Y. Liu, D. Wang, Q. Peng, Q. Zhang, C. Chen and Y. Li, A bimetallic Zn/Fe polyphthalocyanine-derived single-atom Fe-N_4 catalytic site: a superior trifunctional catalyst for overall water splitting and Zn-air batteries, *Angew. Chem., Int. Ed.*, 2018, **57**, 8614–8618.

79 J. Han, J. Bian and C. W. Sun, Recent advances in single-atom electrocatalysts for oxygen reduction reaction, *Research*, 2020, 9512763.

80 K. Liu, X. Zhao, G. Ren, T. Yang, Y. Ren, A. F. Lee, Y. Su, X. Pan, J. Zhang, Z. Chen, J. Yang, X. Liu, T. Zhou, W. Xi, J. Luo, C. Zeng, H. Matsumoto, W. Liu, Q. Jiang, K. Wilson, A. Wang, B. Qiao, W. Li and T. Zhang, Strong metal-support interaction promoted scalable production of thermally stable single-atom catalysts, *Nat. Commun.*, 2020, **11**, 1263.

81 X. Li, Z. Chen, Y. Yang, D. Huan, H. Su, K. Zhu, N. Shi, Z. Qi, X. Zheng, H. Pan, Z. Zhan, C. Xia, R. Peng, S. Wei and Y. Lu, Highly stable and efficient Pt single-atom catalyst for reversible proton-conducting solid oxide cells, *Appl. Catal., B*, 2022, **316**, 121627.

82 Z. Zhang, Y. Chen, L. Zhou, C. Chen, Z. Han, B. Zhang, Q. Wu, L. Yang, L. Du, Y. Bu, P. Wang, H. Yang and Z. Hu, The simplest construction of single-site catalysts by the synergism of micropore trapping and nitrogen anchoring, *Nat. Commun.*, 2019, **10**, 1657.

83 X. He, Y. Deng, Y. Zhang, Q. He, D. Xiao, M. Peng, Y. Zhao, H. Zhang, R. Luo, T. Gan, H. Ji and D. Ma, Mechanochemical kilogram-scale synthesis of noble single-atom catalysts, *Cell Rep. Phys. Sci.*, 2020, **1**, 100004.

84 Z. Khani, M. Taillades-Jacquin, G. Taillades, D. J. Jones, M. Marrony and J. Roziere, Preparation of nanoparticle

core-shell electrolyte materials for proton ceramic fuel cells, *Chem. Mater.*, 2010, **22**, 1119–1125.

85 S. Barison, M. Fabrizio, C. Mortalo, P. Antonucci, V. Modafferi and R. Gerbasi, Novel Ru/$La_{0.75}Sr_{0.25}Cr_{0.5}Mn_{0.5}O_{3-(}$ catalysts for propane reforming in IT-SOFCs, *Solid State Ionics*, 2010, **181**, 285–291.

86 X. Chen and S. P. Jiang, Highly active and stable $(La_{0.24}Sr_{0.16}Ba_{0.6})(Co_{0.5}Fe_{0.44}Nb_{0.06})O_{3-(}$ (LSBCFN) cathodes for solid oxide fuel cells prepared by a novel mixing synthesis method, *J. Mater. Chem. A*, 2013, **1**, 4871–4878.

87 H. Ding and X. Xue, A novel cobalt-free layered $GdBaFe_2O_{5+(}$ cathode for proton conducting solid oxide fuel cells, *J. Power Sources*, 2010, **195**, 4139–4142.

88 S. Choi, T. C. Davenport and S. M. Haile, Protonic ceramic electrochemical cells for hydrogen production and electricity generation: exceptional reversibility, stability, and demonstrated faradaic efficiency, *Energy Environ. Sci.*, 2019, **12**, 206–215.

89 G. Li, H. Jin, Y. Cui, L. Gui, B. He and L. Zhao, Applications of a novel $(Pr_{0.9}La_{0.1})_2(Ni_{0.74}Cu_{0.21}Nb_{0.05})O_{4+(}$ infiltrated $BaZr_{0.1}Ce_{0.7}Y_{0.2}O_{3-(}$ cathode for high performance protonic ceramic fuel cells, *J. Power Sources*, 2017, **341**, 192–198.

90 L. Lei, Z. Tao, T. Hong, X. Wang and F. Chen, A highly active hybrid catalysts modified $(La_{0.60}Sr_{0.40})_{0.95}Co_{0.20}Fe_{0.80}O_{3-(}$ cathode for proton conducting solid oxide fuel cells, *J. Power Sources*, 2018, **389**, 1–7.

91 Y. Huang, F. He, K. Xu, H. Gao, Z. Zhang, Y. Xu, Z. Du, F. Zhu, W. Gong, C. Jian and Y. Chen, Efficient and stable in situ self-assembled air electrodes for reversible protonic ceramic electrochemical cells, *Adv. Funct. Mater.*, 2024, **33**, 2409598.

92 Y. Bu, S. Joo, Y. Zhang, Y. Wang, D. Meng, X. Ge and G. Kim, A highly efficient composite cathode for proton-conducting solid oxide fuel cells, *J. Power Sources*, 2020, **451**, 227812.

93 J. Kim, S. Choi, A. Jun, H. Y. Jeong, J. Shin and G. Kim, Chemically stable perovskites as cathode materials for solid oxide fuel cells: La-doped $Ba_{0.5}Sr_{0.5}Co_{0.8}Fe_{0.2}O_{3-(}$, *ChemSusChem*, 2014, **7**, 1669–1675.

94 Z. Wang, M. Liu, W. Sun, D. Ding, Z. Lv and M. Liu, A mixed-conducting $BaPr_{0.8}In_{0.2}O_{3-(}$ cathode for proton-conducting solid oxide fuel cells, *Electrochem. Commun.*, 2013, **27**, 19–21.

95 J. Kim, S. Sengodan, G. Kwon, D. Ding, J. Shin, M. Liu and G. Kim, Triple-conducting layered perovskites as cathode materials for proton-conducting solid oxide fuel cells, *ChemSusChem*, 2014, **7**, 2811–2815.

96 H. P. Ding, W. Wu, C. Jiang, Y. Ding, W. J. Bian, B. X. Hu, P. Singh, C. J. Orme, L. C. Wang, Y. Y. Zhang and D. Ding, Self-sustainable protonic ceramic electrochemical cells using a triple conducting electrode for hydrogen and power production, *Nat. Commun.*, 2020, **11**, 1907.

97 N. Wang, B. Yuan, C. Tang, L. Du, R. Zhu, Y. Aoki, W. Wang, L. Xing and S. Ye, Machine-learning-accelerated development of efficient mixed protonic-electronic conducting oxides as the air electrodes for protonic ceramic cells, *Adv. Mater.*, 2022, **34**, e2203446.

98 S. Y. Gómez and D. Hotza, Current developments in reversible solid oxide fuel cells, *Renewable Sustainable Energy Rev.*, 2016, **61**, 155–174.

99 W. Wu, H. Ding, Y. Zhang, Y. Ding, P. Katiyar, P. K. Majumdar, T. He and D. Ding, 3D self-architectured steam electrode enabled efficient and durable hydrogen production in a proton-conducting solid oxide electrolysis cell at temperatures lower than 600 °C, *Adv. Sci.*, 2018, **5**, 1800360.

100 C. H. Yang, A. Coffin and F. L. Chen, High temperature solid oxide electrolysis cell employing porous structured $(La_{0.75}Sr_{0.25})_{0.95}MnO_3$ with enhanced oxygen electrode performance, *Int. J. Hydrogen Energy*, 2010, **35**, 3221–3226.

101 Y. Chen, Y. Bu, B. Zhao, Y. Zhang, D. Ding, R. Hu, T. Wei, B. Rainwater, Y. Ding, F. Chen, C. Yang, J. Liu and M. Liu, A durable, high-performance hollow-nanofiber cathode for intermediate-temperature fuel cells, *Nano Energy*, 2016, **26**, 90–99.

102 D. Dong, Y. Wu, X. Zhang, J. Yao, Y. Huang, D. Li, C. Z. Li and H. Wang, Eggshell membrane-templated synthesis of highly crystalline perovskite ceramics for solid oxide fuel cells, *J. Mater. Chem.*, 2011, **21**, 1028–1032.

103 Y. Yang, Y. Wang, Z. Yang, Y. Chen and S. Peng, A highly active and durable electrode with in situ exsolved Co nanoparticles for solid oxide electrolysis cells, *J. Power Sources*, 2020, **478**, 229082.

104 Y. Jiang, L. Ye, S. Zhang and C. Xia, Doped ceria with exsolved Fe^0 nanoparticles as a Sr-free cathode for CO_2 electrolysis in SOECs at reduced temperatures, *J. Mater. Chem. A*, 2022, **10**, 9380–8383.

105 X. Sun, Y. J. Ye, M. Z. Zhou, H. J. Chen, Y. Li, P. R. Chen, D. H. Dong, Y. H. Ling, M. Khan and Y. Chen, Layered-perovskite oxides with *in situ* exsolved Co–Fe alloy nanoparticles as highly efficient electrodes for high-temperature carbon dioxide electrolysis, *J. Mater. Chem. A*, 2022, **10**, 2327–2335.

106 J. Cao, Y. Li, Y. Zheng, S. Wang, W. Zhang, X. Qin, G. Geng and B. Yu, A novel solid oxide electrolysis cell with micro-/nano channel anode for electrolysis at ultra-high current density over 5 A cm^{-2}, *Adv. Energy Mater.*, 2022, **12**, 2200899.

107 P. Priya and N. R. Aluru, Accelerated design and discovery of perovskite with high conductivity for energy applications through machine learning, *npj Comput. Mater.*, 2021, **7**, 90.

108 B. Y. Yuan, N. Wang, C. M. Tang, L. Meng, L. Du, Q. W. Su, Y. Aoki and S. Y. Ye, Advances and challenges in high-performance cathodes for protonic solid oxide fuel cells and machine learning-guided perspectives, *Nano Energy*, 2024, **122**, 109306.

109 S. Zhai, H. Xie, P. Cui, D. Guan, J. Wang, S. Zhao, B. Chen, Y. Song, Z. Shao and M. Ni, A combined ionic Lewis acid descriptor and machine-learning approach to prediction of efficient oxygen reduction electrodes for ceramic fuel cells, *Nat. Energy*, 2022, **7**, 866–875.

110 J. Hyodo, K. Tsujikawa, M. Shiga, Y. Okuyama and Y. Yamazaki, Accelerated discovery of proton-conducting perovskite oxide by capturing physicochemical fundamentals of hydration, *ACS Energy Lett.*, 2021, **6**, 2985–2992.
111 S. Afroze, M. S. Reza, M. R. Amin, J. Taweekun and A. K. Azad, Progress in nanomaterials fabrication and their prospects in artificial intelligence towards solid oxide fuel cells: A review, *Int. J. Hydrogen Energy*, 2024, **52**, 216–247.
112 C. Zhang, Q. Liu, Q. Wu, Y. Zheng, J. Zhou, Z. Tu and S. Chan, Modelling of solid oxide electrolyzer cell using extreme learning machines, *Electrochim. Acta*, 2017, **251**, 137–144.
113 Y. Subramanian, R. Veena, S. A. Muhammed Ali, A. Kumar, R. K. Gubediran, A. Dhanasekaran, D. Gurusamy and K. Muniandi, Artificial intelligence technique based performance estimation of solid oxide fuel cells, *Mater. Today: Proc.*, 2023, **80**, 2573–2576.